CHARACTERIZATION AND CORNEAL TISSUE ENGINEERING APPLICATION OF PEPTIDE AMPHIPHILES

A THESIS

SUBMITTED TO THE MATERIALS SCIENCE AND NANOTECHNOLOGY PROGRAM OF THE GRADUATE SCHOOL OF ENGINEERING AND SCIENCE OF BILKENT UNIVERSITY

IN PARTIAL FULFILLMENT OF THE REQUIREMENTS

FOR THE DEGREE OF

MASTER OF SCIENCE

By

YAVUZ SELİM DAĞDAŞ

August, 2012

I certify that I have read this thesis and that in my opinion it is fully adequate, in scope and in quality, as a thesis of the degree of Master of Science.

……

Assist. Prof. Dr. Ayşe Begüm Tekinay (Advisor)

I certify that I have read this thesis and that in my opinion it is fully adequate, in scope and in quality, as a thesis of the degree of Master of Science.

……

Assoc. Prof. Dr. Mustafa Özgür Güler (Co-Advisor)

I certify that I have read this thesis and that in my opinion it is fully adequate, in scope and in quality, as a thesis of the degree of Master of Science.

……

Assist. Prof. Dr. Fatih Büyükserin

I certify that I have read this thesis and that in my opinion it is fully adequate, in scope and in quality, as a thesis of the degree of Master of Science.

……

Assist. Prof. Dr. Turgay Tekinay

Approved for the Graduate School of Engineering and Science:

……

Prof. Dr. Levent Onural

Director of the Graduate School of Engineering and Science

ABSTRACT

CHARACTERIZATION AND CORNEAL TISSUE ENGINEERING APPLICATION OF PEPTIDE AMPHIPHILES

Yavuz Selim Dağdaş

M.S. in Materials Science and Nanotechnology

August, 2012

Molecular self-assembly is a powerful technique for developing novel nanostructures by using non-covalent interactions such as hydrogen bonding, hydrophobic, electrostatic, metal-ligand, π-π and van der Waals interactions. Hydrogen bonding, hydrophobic and electrostatic interactions promote self-assembly of peptide amphiphile molecules into nanofibers. Bundles of nanofibers form a three-dimensional network resulting in gel formation. Concentration and temperature dependent measurements of gel stiffness suggest that the mechanical properties of the gels are determined by a number of factors including the interfiber interactions and mechanical properties of individual nanofibers. Peptide amphiphile molecules provide a convenient model as extracellular matrix mimetic systems for regenerative medicine studies. Since the substrate stiffness is crucial for cellular

behaviours such as proliferation, adhesion and differentiation, understanding the mechanisms behind the viscoelastic properties of the gels formed by self-assembling molecules can lead to development of new materials with controlled stiffness.

In this study, regeneration of the corneal stroma was used as a model system for utilization of peptide amphiphile molecules in regenerative medicine studies. Corneal stroma is constituted by collagen fiber arrays that are closely packed forming a stiff environment for corneal fibroblasts. The tunability of mechanical properties of self-assembled peptide amphiphile nanostructures was aimed to be utilized in corneal stroma regeneration. Thinning of the corneal stroma is a debilitating problem that can be caused by diseases like keratoconus, infections or accidents. Since corneal stroma has a restricted regenerative capacity, thinning of stroma is usually treated with cornea transplantation, which is limited by the number of donors.

In this thesis, I studied mechanical properties of self-assembled peptide amphiphile nanostructures in nanometer and micrometer scale. I found that the divergence in gel stiffness may arise from the difference of strength of interfiber bonds. An injectable, biocompatible, biodegradable and bioactive system that can be used for thickening the corneal stroma was developed. This system that is composed of nanofibers was observed to enhance viability and proliferation of keratocytes *in vitro*.

Keywords: Peptide amphiphile, self-assembly, nanofibers, cross-link, corneal stroma, regeneration, rheology, AFM, biocompatibility, proliferation, adhesion

ÖZET

PEPTİT AMFİFİLLERİN KARAKTERİZASYONU VE KORNEA DOKU MÜHENDİSLİĞİ UYGULAMASI

Yavuz Selim Dağdaş

Malzeme Bilimi ve Nanoteknoloji Programı, Yüksek Lisans

Tez Yöneticisi: Yard. Doç. Dr. Ayşe B. Tekinay

Ağustos, 2012

Kendiliğinden düzenlenme, hidrojen bağı, hidrofobik, elektrostatik etkileşimler, metal bağı, π-π ve van der Waals bağı gibi bağları kullanarak yeni nano yapıların geliştirilmesinde faydalı bir yöntem olarak uygulanmaktadır. Hidrojen bağı ve hidrofobik ve elektrostatik etkileşimler peptit amfifil moleküllerinin kendiliğinden düzenlenme yoluyla nano fiberler yapmalarını tetiklemektedir. Nano fiberler birbirleri ile etkileşimleri sonucunda üç boyutlu bir ağ oluşturarak jel yapabilmektedirler. Peptit amfifil jellerinin konsantrasyona ve sıcaklığa bağlı mekanik ve yapısal ölçümleri, jel sertliğinin fiberler arası etkileşimlere ve fiberlerin kendi mekanik özelliklerine bağlı olduğunu göstermektedir.

Peptit amfifil molekülleri doğal hücrelerarası matrisi taklit ederek rejeneratif tıp çalışmaları için kullanışlı bir model sunmaktadır. Hücrelerarası ortamın mekanik özellikleri hücrelerin çoğalmasında, yüzeye yapışmasında ve farklılaşmasında

önem arz etmektedir. Kendiliğinden düzenlenme metodu ile oluşturulan jellerin viskoelastik özelliklerinin sebeplerinin bilinmesi gerekli sertlikte yeni malzemelerin geliştirilmesinde fayda sağlayacaktır.

Bu çalışmada peptit amfifil moleküllerinin rejeneratif tıp çalışmalarında kullanımı için model olarak kornea stromasının rejenerasyonu çalışılmıştır. Kornea stroması kollajen fiber dizilerinin sıkı bir şekilde düzenlenmesi ile oluşmuş olup kornea fibroblastları için sert bir ortam oluşturmaktadırlar. Kendiliğinden düzenlenen peptit amfifil molekülleri tarafından oluşturulan nano yapıların mekanik özelliklerinin ayarlanabilir olmaları kornea stroma doku yenilenmesi gibi doku mühendisliği ve rejeneratif tıp çalışmaları için önem arz etmektedir. Keratokonus, enfeksiyonlar veya travmalar sebebiyle korneal stromanın incelmesi korneanın mercek görevini yapmasına engel olabilmektedir. Stromanın kısıtlı miktarda kendini yenileme özelliği sebebiyle, kornea stromasının incelmesi kornea nakli ile çözülmektedir. Hâlbuki enfeksiyon riski ve lazer ile yapılan kornea ameliyatları zaten yetersiz miktardaki nakil için kullanıma uygun kornea sayısını ciddi anlamda azaltmaktadır.

Bu tezde, kendiliğinden düzenlenme ile peptit amfifil moleküllerince oluşturulan nano yapıların mekanik özellikleri nano ve mikro düzeyde incelenmiştir. Sonuç olarak peptit amfifil molekülleri tarafından oluşturulan jellerin sertliklerinde görülen değişikliklerin fiberler arası etkileşimlerin farklı olmasından kaynaklandığı bulunmuştur. Bunun yanında, kornea stroma dokusunun kendini yenilemesi ve kalınlaşması için enjekte edilebilen, biyoaktif, biyouyumlu ve

biyobozunur bir malzeme geliştirilmiştir. Geliştirilen malzemenin kornea fibroblastlarının canlılıklarını ve çoğalma miktarlarını arttırdığı gözlemlenmiştir.

Anahtar Kelimeler: Peptit amfifil, kendiliğinden düzenlenme, nano fiber, çaprazlama, reoloji, AFM, kornea stroması, biyouyumluluk, hücre çoğalması, hücre bağlanması

ACKNOWLEDGEMENT

I would like to express my gratitude to my supervisors Assist. Prof. Dr. Ayşe Begüm Tekinay and Assist. Prof. Dr. Mustafa Özgür Güler for their guidance, moral support, and assistance during this research.

I would like to thank my brother Yasin Fatih Dağdaş for all his support that has been invaluable for me.

I would like to thank to Ayşegül Tombuloğlu, Zeliha Soran, Hilal Ünal and Turan Selman Erkal for their partnership in this research.

I would like to express my special thanks to Assoc. Prof. Dr. Aykutlu Dana, Dr. Bahri Aydın and Dr. Ahmet Hondur for their support and sharing their knowledge.

I want to thank all current and former members of the Nanobiotechnology and Biomimetic Materials group for providing a high standard scientific environment. It was wonderful to work with them.

I would like to thank Rashad Mammadov, Ruslan Garifullin and Turan Selman Erkal for their friendship and support that helped to keep my spirits high all the time which I appreciate very much.

I would like to thank UNAM (National Nanotechnology Research Center) and TÜBİTAK (The Scientific and Technological Research Council of Turkey) grant number 110M355 for financial support.

LIST OF ABBREVIATIONS

PA:	Peptide Amphiphile
ECM:	Extracellular Matrix
FMOC:	9-Fluorenylmethoxycarbonyl
HBTU:	2-(1H-Benzotriazol-1-yl)-1,1,3,3-tetramethyluronium hexafluorophosphate
DIEA:	N, N-Diisopropylethylamine
DMF:	Dimethylformamide
TFA:	Trifluoroacetic Acid
LC-MS:	Liquid Chromatography-Mass Spectrometry
AFM:	Atomic Force Microscopy
TEM:	Transmission Electron Microscopy
FT-IR:	Fourier Transform Infrared Spectroscopy
SEM:	Scanning Electron Microscopy
CD:	Circular Dichroism
ITC:	Isothermal Titration Calorimetry
SPSS:	Solid Phase Peptide Synthesis

TABLE OF CONTENTS

LIST OF FIGURES

LIST OF TABLES

CHAPTER 1

Interfiber interactions alter stiffness of gels formed by supramolecular self-assembled nanofibers

This work was partly published in "Interfiber Interactions Alter Stiffness of Gels Formed by Supramolecular Self-Assembled Nanofibers" **Yavuz S. Dagdas**, Aysegul Tombuloglu, Ayse B. Tekinay, Aykutlu Dana and Mustafa O. Guler *Soft Matter*, 2011, 7, 3524-3532 " Reproduced (or 'Reproduced in part') with permission from Royal Society of Chemistry.

Introduction

Over the last century, the developments observed in medicine have contributed to the quality of human life and has increased life span significantly. The increase in the human life span and quality resulted in new challenges for medicine like age-related or degenerative diseases. The developments in nanotechnology and its use in biological sciences have lead to the emergence of a new interdisciplinary science, "bionanotechnology". The use of nanoscience for biology and medicine has found a wide range of applications for different areas like drug delivery, regenerative medicine and tissue engineering. The first examples of nanomedicine were mainly based on the enhanced delivery of existing drugs with nanostructures for increasing their efficiency.However the efficiency of these nanostructures depends on controlled development of structure and function.

Self-assembled nanostructures have extensively been used in various applications where nanoscale properties have important effects on function. These nanostructures are usually formed by small molecules through non-covalent interactions and the assembly mechanisms are sensitive to changes in the environment [1-3]. Peptide amphiphile (PA) molecules self-assemble into nanofibers under controlled conditions. Self-assembly of PA molecules is mainly controlled by hydrogen bonding (peptide segment) [4] and hydrophobic forces (alkyl tail) [5]. Amino acids in the PA molecules direct β-sheet formation through hydrogen bonding and the alkyl tail in the PA molecules direct sphere formation through hydrophobic collapse in aqueous environment. Peptide segment in PA molecules form a network of hydrogen bonds after charge

neutralization through either electrolyte addition or pH change, and directs formation of nanofiber-like cylindrical micelles instead of spherical micelles [2, 4, 6-9]. The PA nanofibers form a 3-D network resulting in gel formation in aqueous conditions [3-4, 10-13].

The nanofiber networks formed by PA molecules are utilized as scaffolds for tissue engineering due to their ability to mimic native extracellular matrix (ECM) [8, 13-16]. ECM supports attachment, proliferation and migration of cells and provides mechanical support to tissue. The mechanical properties of surroundings of cells can result in alterations in cellular responses through cytoskeletal structure, thus affecting the cell behavior and direct stem cell differentiation [17-19]. Therefore, for tissue engineering applications, it is essential to control mechanical features of the scaffolds as well as their bioactivity. In the current study, solid phase peptide synthesis method was utilized for the synthesis of peptide amphiphile molecules.

1.1 Solid Phase Peptide Synthesis

Solid phase peptide synthesis (SPSS) was first developed by Bruce Merrifield for the synthesis of polypeptides and received Nobel Prize in 1984. This method has advantages in terms of efficiency and purity of products over the conventional synthesis methods. It is not as labor intensive as liquid phase synthesis method especially for longer sequences. Dr. Merrifield used benzyloxycarbonyl and t-butoxycarbonyl protected amino acids for the synthesis of polypeptides. Number of different protecting groups, solvents and reagents have been developed and used for this method and 9-fluorenylmethoxycarbonyl (Fmoc) group protected amino acids were used within this study.

The synthesis of peptides by SPSS method starts with loading of protected amino acids on polymeric supports named as resin. There are commercially available resins already loaded with amino acids with protecting groups. The principle of SPPS is based on repetitive cycles of deprotection and coupling. The protected N-terminal amine of resin attached peptide is deprotected resulting in free N-terminal amine which is coupled with another amino acid later on. After completion of amino acid addition, peptide is cleaved from the resin with all side chain protecting groups leaving a free crude peptide. Peptides are purified after the cleavage usually with reverse phase HPLC.

In this study, SPSS method was utilized in order to synthesize peptide amphiphile molecules with an aim to use them for regenerative medicine studies as extracellular matrix mimetic materials. The mechanical properties of these nanofiber systems are of importance, since they are crucial for mediating cellular responses.

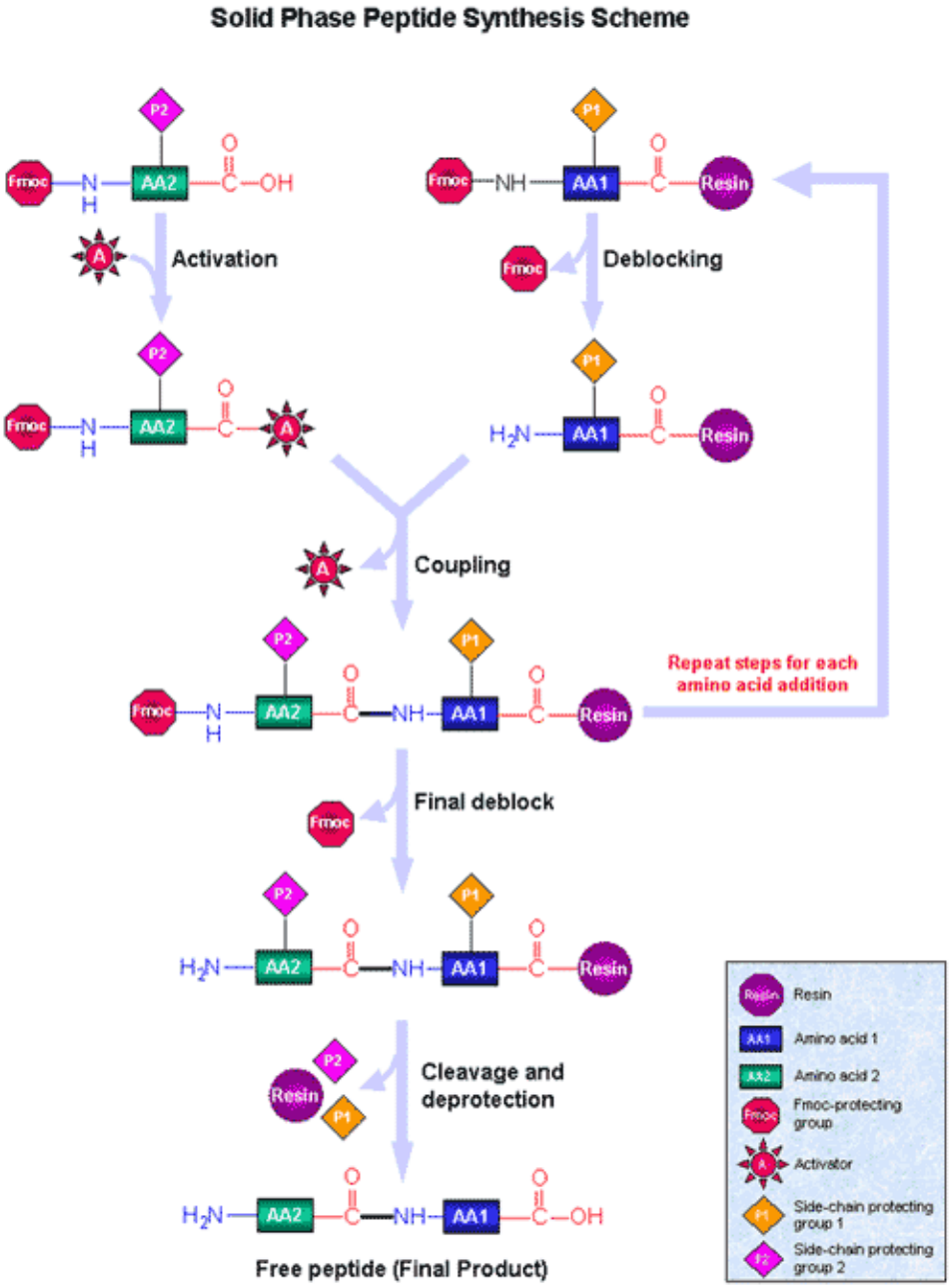

Figure 1. Solid Phase Synthesis Diagram. Reproduced with permission from Sigma-Aldrich.

1.2 Effect of Substrate Stiffness on Cell Behaviour

Tissues are made up of cells and extracellular space that is filled with a complex network of macromolecules forming the extracellular matrix (ECM). There is a dynamic interaction between cells and ECM that direct tissue morphogenesis. The direct interaction between cell and ECM by means of receptor signaling and the indirect role of ECM on the controlled mobilization of growth or differentiation factors are known to affect cellular functions, cell proliferation and phenotype [20-22]. In addition to the roles of ECM on chemical signaling, its physical properties also affect cellular behaviours such as motility [23], phagocytosis [24] and differentiation [17].

Mechanical features of PA gels can be tuned for various tissue engineering approaches depending on tissue type. The PA molecules form a dynamic assembly which is affected by pH change, electrolyte addition and electrostatic interactions. Thus, a better understanding of gelation mechanisms of PA molecules will help us design appropriate substrates for tissue engineering studies. The self-assembled PA nanostructures differ from traditional polymeric materials in terms of 3-D interactions. The mechanical properties of the networks formed by polymeric nanostructures are directly related to material concentration [25-26]. Increase in the concentration results in extension of the nanostructures and the interaction between the nanostructures results in enhanced stiffness in microscale. Due to their dynamic nature, the microscale mechanical properties of the PA based networks are not affected by interactions among the nanostructures in a similar fashion to polymeric systems. Therefore,

it is important to understand the relationship between the nano and micro scale mechanical properties of self-assembled PA materials.

Materials and Methods

2.1 General Methods

The identity of the peptide amphiphiles were assessed by Agilent 6530-1200 Q-TOF LC/MS equipped with ESI-MS and a Zorbax Extend C18 column (Agilent 4.6 x 100 mm, 3.5 μm). The purification of the PA molecules were performed with reverse-phase HPLC system with Zorbax Extend-C18 21.2 x 150 mm column for basic conditions. A: 0.1 % ammonium hydroxide in water and B: 0.1% ammonium hydroxide in acetonitrile gradient was used for analytical and preparative HPLC. Amide bond was observed at 220 nm.

2.2 Materials

9-Fluorenylmethoxycarbonyl (Fmoc) protected amino acids, Fmoc-Asp-(OtBu)-Wang resin and 2-(1H-Benzotriazol-1-yl)-1,1,3,3-tetramethyluronium hexafluorophosphate (HBTU) were purchased from NovaBiochem and ABCR. The other chemicals were purchased from Fisher, Merck, Alfa Aesar or Aldrich and used as received, without any purification.

2.3 Synthesis of Peptides

Peptide amphiphile (PA) molecules were synthesized by using fluorenylmethoxycarbonyl (Fmoc) chemistry. Synthesis was performed manually on a 0.25 mmole scale using a 50 ml peptide synthesis vessel on a wrist action shaker. PA molecules were synthesized by using Fmoc-Asp-(OtBu)-Wang resin. After each reaction, resin was washed three times with DMF, DCM and DMF respectively. All amino acids were activated by adding 2 molar equivalents of amino acid to 1.95 equivalents of O-Benzotriazole-

N,N,N',N'-tetramethyl-uronium-hexafluoro-phosphate (HBTU) and dissolved in 10 ml of DMF. After complete dissolution of amino acid and HBTU in DMF, 3 molar equivalents of *N*-ethyl-diisopropylamine (DIEA) were added into the solution. The solution was mixed thoroughly and kept for 3 minutes before adding to resin. Each coupling reaction was performed for 2.5 h. For each coupling reaction, Fmoc groups were removed by shaking resin in 20% piperidine in N,Ndimethylformamide (DMF) for 20 min. The alkylation reaction was performed by coupling with lauric acid. Lauric acid coupling was performed same as amino acid coupling using lauric acid instead of amino acid. A ninhydrin test was performed after the addition of each amino acid and after the addition of the fatty acid. When the ninhydrin test yielded positive results, the coupling reaction was repeated; otherwise 10 ml of 10% acetic anhydride in DMF was added and resin was shaken for 30 min. Peptide cleavage from resin and deprotection were performed with 95:2.5:2.5 trifluoroacetic acid (TFA): triisopropylsilane (TIS): water for 2.5 h at room temperature. After the cleavage reaction, PA molecules were collected in a clean round bottom flask and washed several times with DCM. The collected solution was rotary-evaporated. After evaporation, ice-cold diethyl ether was added and was left at -20 °C overnight. The PA-diethyl ether mixture was collected in 50 ml falcon tubes and centrifuged at 8000 rpm for 25 min. Supernatant was decanted and the remaining diethyl ether was evaporated. The pellet was dissolved in deionized H_2O at a resistance of 18.2 Ω and was freeze-dried.

2.4 Characterization of Peptide Amphiphiles

2.4.1 Scanning Electron Microscopy (SEM)

The nanofiber networks formed by the PA molecules were observed with scanning electron microscopy (SEM). SEM samples of the PA-HCl gels and the PA-$CaCl_2$ gels were prepared at final PA and gelator concentrations of 8.3 mM and 41.7 mM respectively. The PA-HCl samples had a final pH of 2 and the PA-$CaCl_2$ gels were mixed at 1:5 molar ratios. The formed gels were then placed onto a metal mesh and dehydrated with increasing concentrations of ethanol up to 100%. The ethanol was then removed by critical point drying (Tourismis, Autosamdri-815B). Samples were sputter-coated twice with 2.5 nm of Pt to ensure complete coating. Visualization of the nanofiber networks were carried out with a FEI, Nova NanoSEM 430 at 18 kV with an average working distance of 5 milimeters.

2.4.2 Transmission Electron Microscopy (TEM)

Two different sample formulations were prepared for TEM; the mixture of PA molecules with $CaCl_2$ or with HCl. 10 µl of 2 mM PA solution at pH 7 was mixed with 2 µl of 250 mM $CaCl_2$ solution and 10 µl of 2 mM PA solution at pH 7 was mixed with 2 µl of 250 mM HCl solution. PA with $CaCl_2$ and PA with HCl solutions were cast on TEM grids and incubated for 3 minutes. Samples were stained with 2% aqueous uranyl acetate solution and air dried overnight. TEM images were acquired with a FEI Tecnai G2 F30 TEM at 100 kV.

2.4.3 Atomic Force Microscopy (AFM)

AFM samples were prepared on 1 cm^2 silicon wafers (with low residual roughness (<1 nm/μm^2)) using 25 µl of 0.5 mM PA solutions. PA–$CaCl_2$ samples were prepared by mixing 100 µl of 0.5 mM PA solution at pH 7 with 3 µl of 50 mM $CaCl_2$ solution (1:3 molar ratio). PA with HCl samples were prepared by adjusting the final pH to 2. After addition of $CaCl_2$ and HCl to pH 7 PA solution, eppendorfs were vortexed thoroughly and sonicated for 5 min. 1 min after casting the solution onto a silicon wafer, excess water was removed with a tissue and the sample was air dried. Dynamic mode imaging was used to image the topography of the resulting samples, using appropriate cantilevers (cantilever stiffness of k=3-40 N/m, resonance frequency of f_0=70-350 kHz for the dynamic mode).

2.4.4 Circular Dichroism (CD) at room temperature

CD spectra of the PA solutions were obtained using a J-815 Jasco spectrophotometer in the far UV region (190 – 300 nm) using quartz cuvettes of 1 mm path length. Room temperature CD studies involved samples that are prepared from same batch and pH was adjusted to 7 before use. Spectra were acquired for three formulations; PA at pH 7, PA mixed with $CaCl_2$ and PA mixed with HCl. The PA with HCl sample was prepared by adjusting the pH to 2 by addition of HCl and the PA with $CaCl_2$ sample was prepared by adding $CaCl_2$ at 1:5 molar ratios compared to the PA to ensure complete neutralization of the charges at pH 7. A solution of 0.1 mM PA was prepared in deionized water and the pH was adjusted to 7. For the PA-$CaCl_2$ measurements 5 µl of 100 mM $CaCl_2$ was added to 1 ml of PA solution. For the PA-HCl measurements,

the pH of a 1 ml sample of the PA was adjusted to pH 2 with HCl. Averages of three scans of each sample were taken.

In order to study the effect of $CaCl_2$ on secondary structure formation, CD spectra were monitored after adding EDTA to the PA-$CaCl_2$ sample. 2.6 ml of 7 mM $CaCl_2$ was added to 400 µl of a 1.05 mM solution of PA and incubated at room temperature for 6 h before acquiring CD spectra. 10 µl of 0.05 M EDTA was then added to the solution and further spectra were acquired immediately and again after a 6 h incubation. CD spectra were obtained from 190 nm to 300 nm at a digital integration time of 1 s, a band width of 1 nm and a data pitch of 0.1 nm.

2.4.5 Circular Dichroism at variable temperatures

Variable temperature CD studies were carried out with Jasco J-815 equipped with PTC-423S/15 peltier unit. Before preparing samples, 1.05 mM PA was sonicated for an hour. For preparing low pH samples PA was diluted in sodium acetate buffer or HCl. PA/$CaCl_2$ samples were prepared by diluting PA in Tris buffer containing $CaCl_2$. Details can be followed from the table given in Table 1. Samples were mixed well and incubated for 24 h at room temperature for equilibration. For each measurement, 300 µl of sample was pipetted into a 1 mm quartz cuvette which was inverted gently for mixing without damaging any assembled structures. CD spectra were obtained from 190 nm to 300 nm at a digital integration time of 4 s, a band width of 1 nm and a data pitch of 0.1 nm. Samples were heated at a rate of 0.2 °C/min, and spectra were collected at 1 ˚C intervals between 25 ˚C and 90 ˚C. After acquisition, spectra were smoothed

with means movement with a convolution width of 15, which was included in Spectra-Manager (Jasco-UK ltd) software.

2.4.6 Fourier Transform Infrared Spectroscopy

Three different sample formulations were prepared for FTIR: PA solution at pH 7, PA solution mixed with $CaCl_2$ and PA solution mixed with HCl. PA at pH 7 sample was prepared by using 150 µl of 10 mM PA solution. PA with $CaCl_2$ sample was prepared by mixing 125 µl of 10 mM PA solution with 25 µl of 1 M $CaCl_2$. PA with HCl sample was prepared by mixing 125 µl of 10 mM PA solution with 25 µl of 1 M HCl. In order to obtain complete diffusion of gelling agents, samples were shaken overnight and then frozen and lyophilized. 1 mg of each formulation was mixed with 100 mg of KBr and crushed thoroughly. Transmittance of the pellet was measured by Bruker, Vertex 70 FT-IR instrument.

Table 1. Sample preparation chart for circular dichroism studies at variable temperatures

Sample	**Starting concentration of PA**	**Diluted within**	**Final concentration of PA**	**Final concentration of buffer & pH**	**Final concentration of $CaCl_2$**
PA/Acetate buffer	1.05 mM	2.055 mM Sodium acetate buffer	0.028 mM	2 mM Sodium acetate buffer (pH 3.6)	-
PA/HCl	1.05 mM	10.3 mM HCl	0.028 mM	pH 2	-
PA/Tris + $CaCl_2$	1.05 mM	11.5 mM Tris buffer + 0.807 mM $CaCl_2$	0.14 mM	10 mM Tris buffer (pH 7.4)	0.7 mM
PA/Tris + $CaCl_2$	1.05 mM	11.5 mM Tris buffer + 0.231 mM $CaCl_2$	0.14 mM	10 mM Tris buffer (pH 7.4)	0.2 mM

2.4.7 Zeta Potential and pH Titration

Zeta potential measurements were performed with Malvern Nano-ZS zetasizer which contains a pH meter and titration system. Three formulations were used for zeta potential samples. PA at pH 7, PA at pH 2 and PA at pH 7 with $CaCl_2$. PA solutions were prepared at 0.05 wt % and pH was adjusted to 7 before use. PA with $CaCl_2$ was at 1:5 molar ratio respectively and pH was adjusted with 0.1 M HCl for PA at pH 2 sample. 0.06 wt % PA solution was prepared for pH titration study and pH was adjusted to 11 before use. pH titration was done by adding 0.1 M HCl to the PA solutions. Smoluchovski method was used to determine the zeta potential values.

2.4.8 Oscillatory Rheology

Rheology measurements were performed with an Anton Paar Physica RM301 Rheometer operating with a 25 mm parallel plate at 0.5 mm gap distance. Freeze-dried peptide amphiphile molecules were dissolved in deionized water and pH was adjusted to 7 with 0.1 M NaOH solution. The total volume of each sample was set to 150 µl and gel formation was achieved by mixing 125 µl of peptide amphiphile solution (pH 7) with 25 µl of aqueous gelator solution (HCl or $CaCl_2$). The gel was prepared on the lower plate of the rheometer and gelling agents were added dropwise in order to prevent any deformation on gel structure with a mole excess amount to ensure higher diffusion rate and improved interaction with PA molecules. Four different concentrations of PA and gelator were investigated using time sweep oscillatory measurements. Final concentration of PA and gelators are listed in Table 2. The stage temperature was adjusted to 25 °C and all samples were allowed to

equilibrate for 15 min before measurement to achieve stable gel formation. Wet tissue paper was placed inside the chamber around the edge of the plate to provide a humid environment preventing solvent evaporation from the sample during the experiments. Measurements were performed for 60 min at 10 rad/s and 0.5% strain.

Temperature dependent oscillatory rheology was performed for PA-HCl and PA-$CaCl_2$ gels with final concentrations of 8.5 mM PA with 833.3 mM gelator. Measurements were performed from 25 °C to 85 °C at a heating rate of 1 °C/min with a 10 rad/s frequency and 0.5 % strain.

Table 2. Concentration of PA and gelator (HCl or $CaCl_2$) for different time sweep rheology experiments.

Initial PA Concentration (mM)	**Final PA Concentration (mM)**	**Initial Gelator Concentration (mM)**	**Final Gelator Concentration (mM)**
20	16.9	2000	1666.7
10	8.5	1000	833.3
5	4.2	500	416.7
2.5	2.1	250	208.3

Results and Discussions

3.1 Design and Synthesis of Peptide Amphiphiles

The PA molecule used during the study in this chapter is composed of an alkyl tail, β-sheet forming (VVAG) peptide sequence followed by a glutamic acid residue, which is effective in increasing the solubility of the molecule and a bioactive epitope (RGD), a peptide sequence that enhances cell adhesion (Figure 2) [27]. The PA molecule was synthesized and purified with Agilent 6530-1200 Q-TOF LC/MS equipped with ESI-MS and a Zorbax Extend C18 column. (Figure 3 and Figure 4).

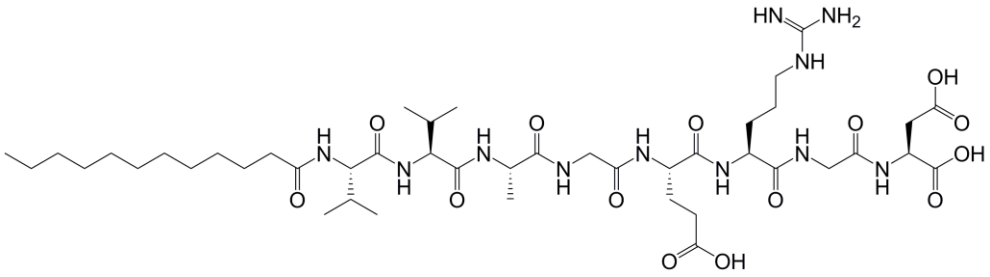

Figure 2. Chemical structure of the investigated peptide amphiphile molecule.

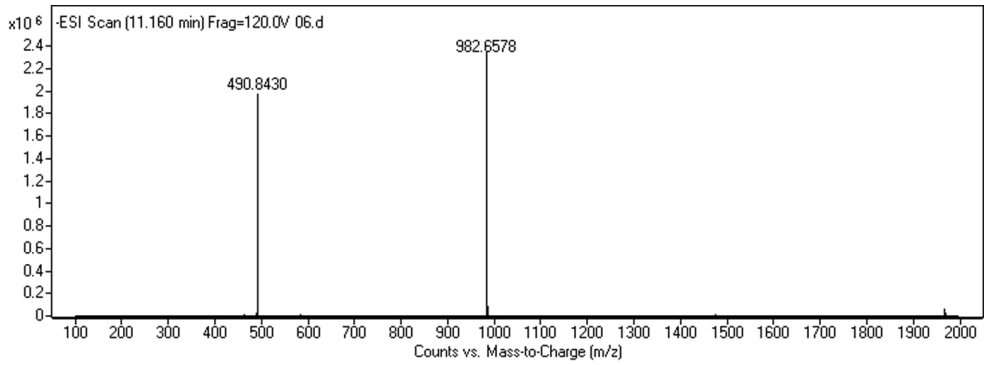

Figure 3. Electrospray ionization mass spectra of the PA. $(M-H)^{-1}_{observed}$+= 982.65, $(M-H)^{-1}_{calculated}$+= 982.57, $(M-2H)/2^{-1}_{observed}$+=490.84, $(M-H)^{-1}_{calculated}$+= 490.78

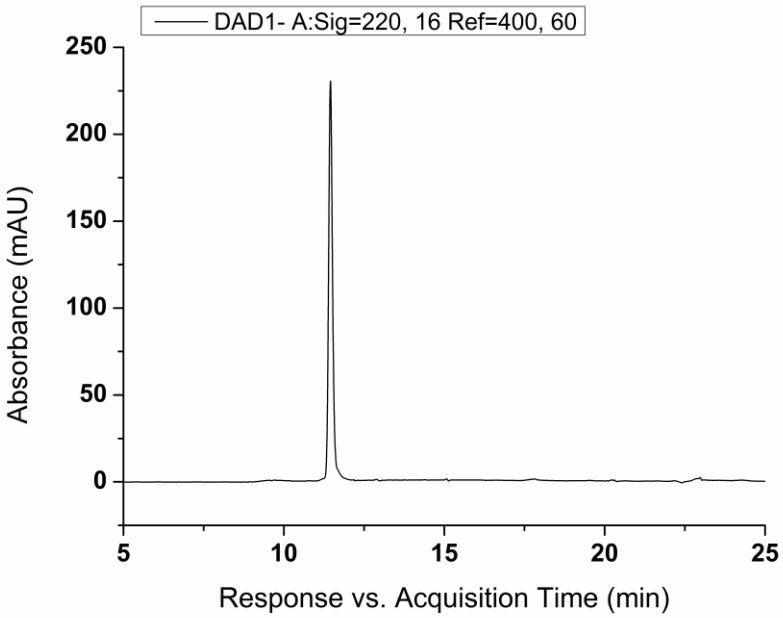

Figure 4. Analytical HPLC trace of the PA.

3.2 Morphology of Peptide Amphiphile Nanofibers

Nanoscale morphology of the PA nanofibers was observed by SEM. The nanofiber networks formed by PA nanofibers through $CaCl_2$ or HCl addition are shown in Figure 5a and Figure 5b, respectively. The PA nanofibers formed bundles which were favored by interfibrillar interactions mediated by hydrogen bonding, electrostatic attractions between positively and negatively charged amino acids and ion bridging formed by calcium ions. As a result of SEM imaging, no significant differences in bundle and mesh size were observed between the nanofiber network and PA nanofibers formed through either mechanism.

PA nanofibers formed by addition of $CaCl_2$ or HCl were visualized by transmission electron microscopy (TEM) and atomic force microscopy (AFM). TEM revealed that PA with $CaCl_2$ and PA with HCl nanofibers are around 8-10 nm in diameter and several micrometers in length (Figure 5c and Figure 5d respectively). AFM results indicated that PA molecules have formed nanofibers in several lengths for both self-assembly mechanisms. However, it is noteworthy that PAs with $CaCl_2$ samples contain longer fibers whereas PAs with HCl samples contain shorter but more aggregated fibers arranged as bundles. Even though the PA-HCl and the PA-$CaCl_2$ samples are quite similar in SEM figures, they show significant differences in AFM images. This difference is mostly due to the formation of PA nanofiber bundles during drying of AFM samples.

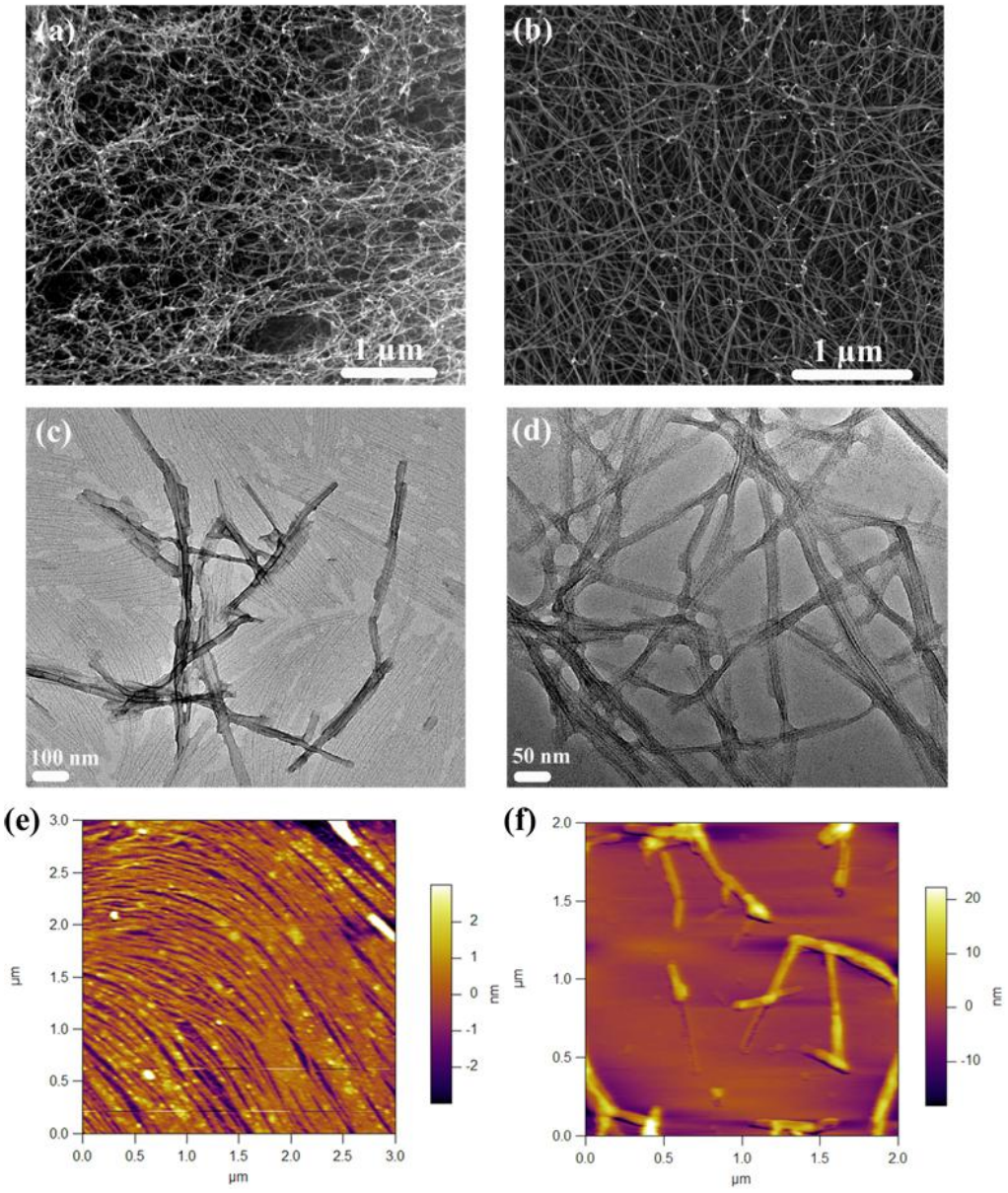

Figure 5. Scanning electron micrographs of the PA nanostructures demonstrating entangled fiber bundles. (a) PA with $CaCl_2$ gel formed with 10 mM PA and 100 mM $CaCl_2$ (b) PA with HCl gel formed with 10 mM PA and 100 mM HCl (scale bar 1µm). Transmission electron micrographs of (c) PA with $CaCl_2$ gel and (d) PA with HCl gel. AFM topography micrographs of (e) PA with $CaCl_2$ gel and (f) PA with HCl gel.

3.3 Circular Dichroism Spectra of Peptide Amphiphiles at Room Temperature

The effect of peptide secondary structure on the self-assembly process was studied by circular dichroism (CD) spectroscopy. Previous studies demonstrated that the cylindrical micelles formed by PA molecules contain β-sheets and that amino acids which are closer to the hydrophobic tail are considered to be critical for β-sheet secondary structure [7]. The effect of the self-assembly process on the secondary structure was studied with CD spectroscopy. The CD experiments were carried out at room temperature and at variable temperatures. Three different formulations were studied; PA at pH 7, PA with $CaCl_2$ and PA with HCl. The PA at pH 7 was analyzed to determine whether the PA molecules self-assemble into defined secondary structures without any charge screening. The PA with HCl sample was studied in order to see the effect of pH change on the secondary structure formation of the PA nanofibers. The PA with $CaCl_2$ formulation was studied to observe the effect of electrolyte addition without any pH change on secondary structure.

In CD spectra, the spectrum for random coil displays a small positive peak at approximately 230 nm and a large single peak at approximately 195 nm whereas β-sheet displays a negative band approximately at 220 nm and a positive band at 195 nm. Figure 6a shows the CD spectra of the PA at pH 7, PA with $CaCl_2$ and PA with HCl samples. The CD studies revealed that both self-assembly mechanisms, either through pH change or electrolyte addition, resulted in predominantly β-sheet signals. However, the PA solution at pH 7 revealed

random coil signal. These results show that the PA molecules do not self-assemble into defined secondary structures at physiological pH without charge screening ($CaCl_2$) or charge neutralization (HCl). Addition of a divalent cation, Ca^{2+} or lowering the pH causes charge screening (Ca^{2+}) and charge neutralization (H^+) of these molecules. Charge screening and neutralization of PA molecules eliminate the repulsive forces and enable formation of hydrogen bonding networks. Formation of hydrogen bonding networks together with hydrophobic collapse of alkyl tail leads to formation of self-assembled structures [28]. Charge screening (Ca^{2+}) and charge neutralization (H^+) of the PA molecules have been studied by measuring the zeta potential of the three formulations (Figure 7a). The PA molecules at pH 7 were neutralized by addition of $CaCl_2$ (1:5 molar ratio) or adjusting pH to 2. pH dependent charge neutralization of PA molecules is shown in Figure 7b. The CD and zeta potential data suggest that neutralization of the PA molecules leads to aggregation of these molecules and formation of β-sheet secondary structure. Thus, neutralization of charges enables PA molecules to self-assemble into defined nanostructures. Addition of EDTA to the PA with $CaCl_2$ sample destroyed the β-sheet assembly and resulted in random coil signals in CD spectrum due to the removal of Ca^{2+} ions from the solution (Figure 8). Charge screening (Ca^{2+}) and charge neutralization (H^+) is mainly brought about by dynamic interactions which can be reversed by isolation of neutralizers from the environment.

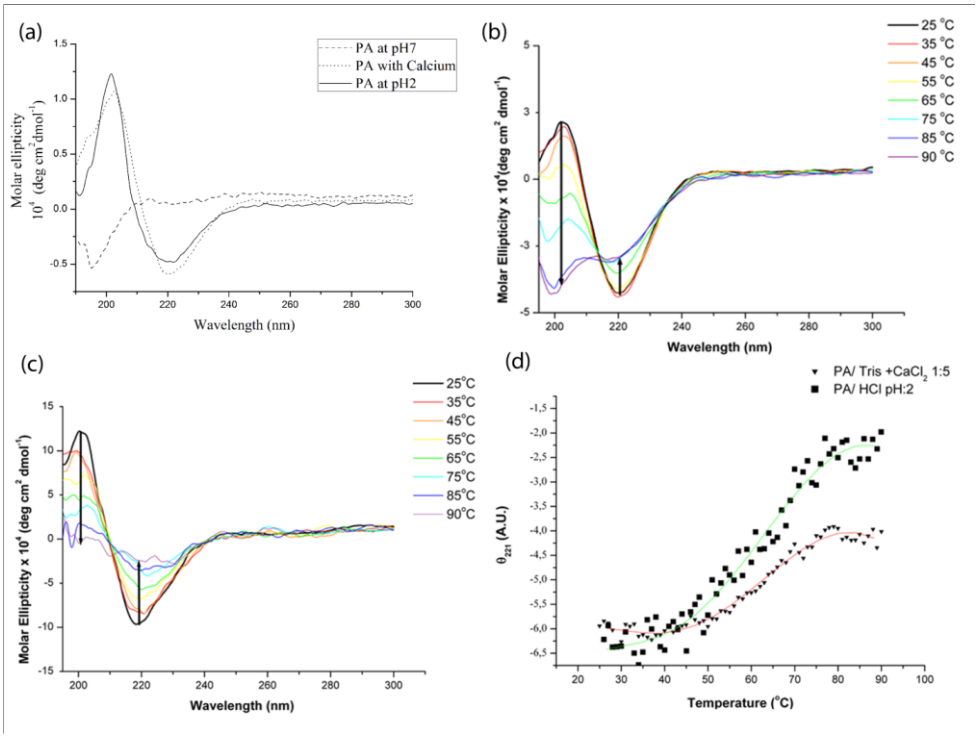

Figure 6. Circular dichroism spectra of the PA (a) at pH 7, PA at pH 2 and PA with $CaCl_2$ at room temperature. Circular dichroism spectra of (b) PA with $CaCl_2$ (1:5 molar ratio), (c) PA with HCl (pH 2) between 25 ºC and 90 ºC. (d) Ellipticity at 221 nm for PA with $CaCl_2$ (1:5 molar ratio) and PA with HCl (pH 2) monitored between 25 ºC and 90 ºC.

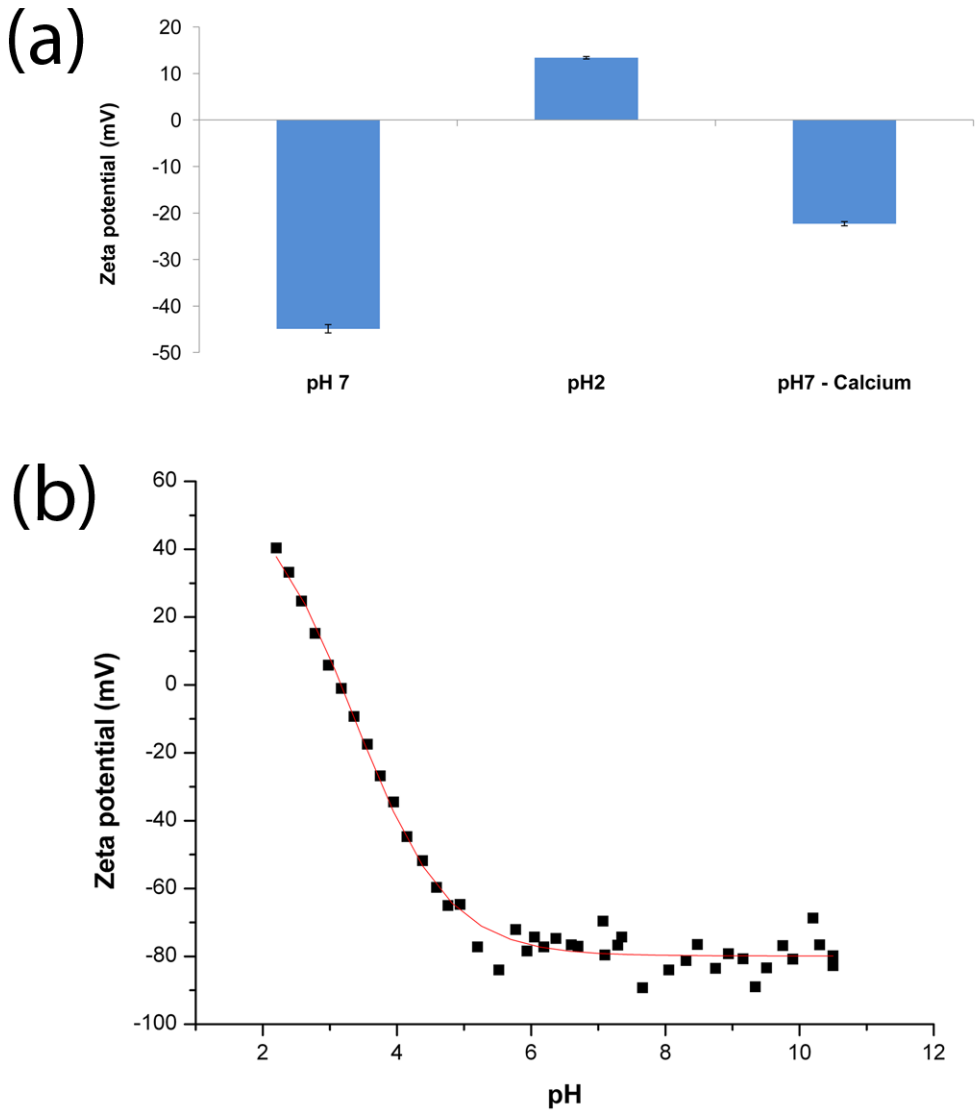

Figure 7. (a)Zeta potential graph of the PA at pH 7, pH 2 and pH 7 with $CaCl_2$, (b) zeta potential change with pH.

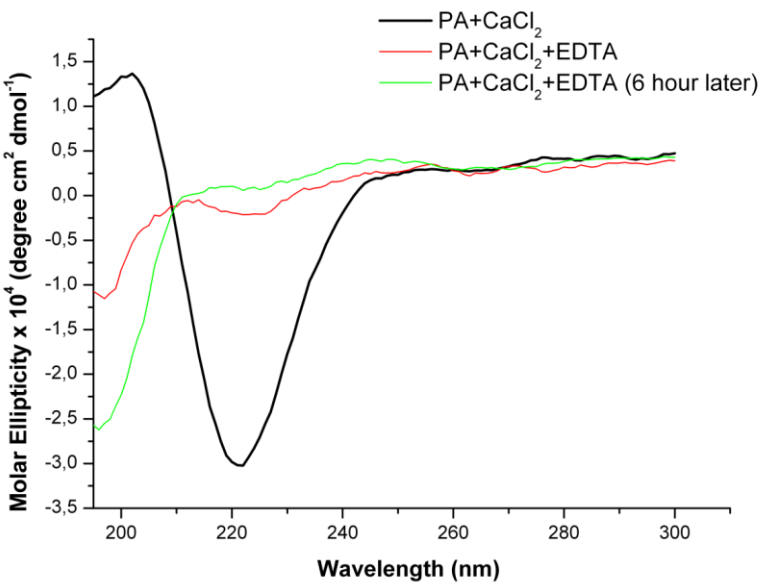

Figure 8. The PA with $CaCl_2$, addition of EDTA disturbs β-sheet structure immediately, after 6 h random coil becomes the most predominant secondary structure.

3.4 Fourier Transform Infrared Spectroscopy of Peptide Amphiphiles

FT-IR spectroscopy was also used for the analysis of the three formulations (pH 7, pH 2 and pH 7 with calcium ions) used in the CD experiments. FT-IR spectra for all three formulations exhibit an amide I peak at 1633 cm^{-1} which is typical for β-sheets [29] (Figure 9). Although a β-sheet signal is expected from samples of pH 2 and pH 7 with calcium ions, the pH 7 sample also exhibited β-sheet. It is likely that β-sheet signal observed in pH 7 sample is due to the stacking and close packing of the PA molecules during lyophilization process. These results suggest that both FT-IR and CD experiments reveal consistent results, indicating effect of pH screening and addition of divalent cations on secondary structure of the PA molecules.

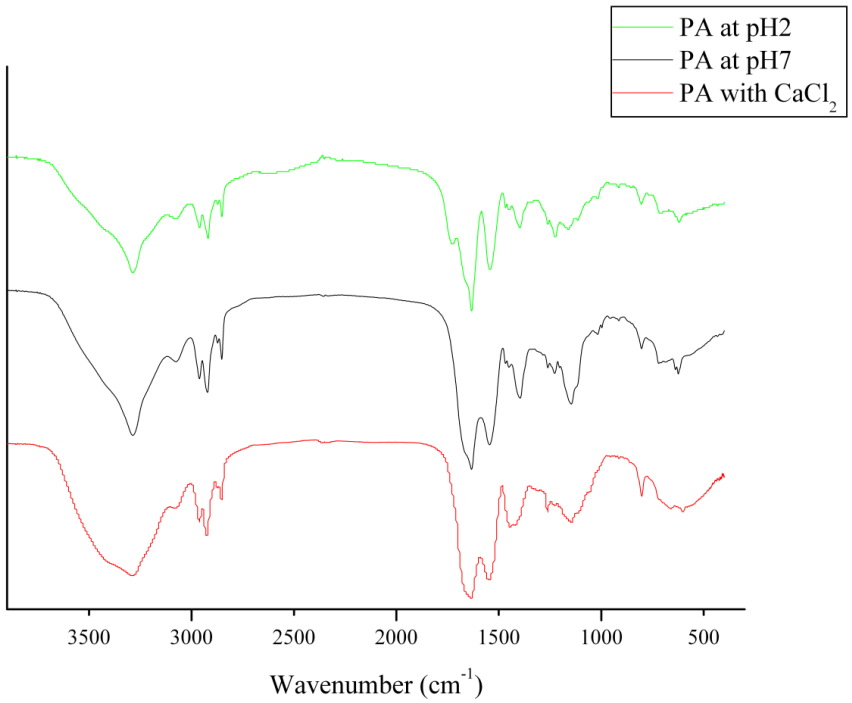

Figure 9. FTIR spectra of lyophilized PA with $CaCl_2$, PA with HCl, PA at pH 7.

3.5 Circular Dichroism Spectra of Peptide Amphiphiles at Variable Temperatures

Variable temperature CD studies enabled monitoring of the thermal denaturation of the β-sheet secondary structure triggered by $CaCl_2$ addition or lowering the pH. At 25 ˚C, characteristic β-sheet traces with negative bands at about 220 nm and positive bands around 202 nm were observed for $CaCl_2$ and pH 2 samples. The β-sheet signals gradually diminished while heating from 25 ˚C to 90 ˚C indicating denaturation of peptide assemblies formed by β-sheet composed of hydrogen bonding, Figure 6b and Figure 6c. Both $CaCl_2$ and pH 2 samples exhibited similar melting profiles with melting temperatures at around 60-65 ˚C (Figure 6d). At pH 3.6 and in the presence of 1.43 molar equivalent of $CaCl_2$, the CD spectra at room temperature possess red shifted bands and strong signals at π-π* transition region (Figure 10a, Figure 10b) which may additionally indicate β-sheets existing in twisted conformation rather than planar in these samples [30]. At pH 3.6, the PA molecules are partially neutralized for charges (Figure 11). At this particular pH and $CaCl_2$ concentration full charge screening does not occur and so electrostatic interactions may be fomenting PAs to become assembled in twisted β-sheet conformation.

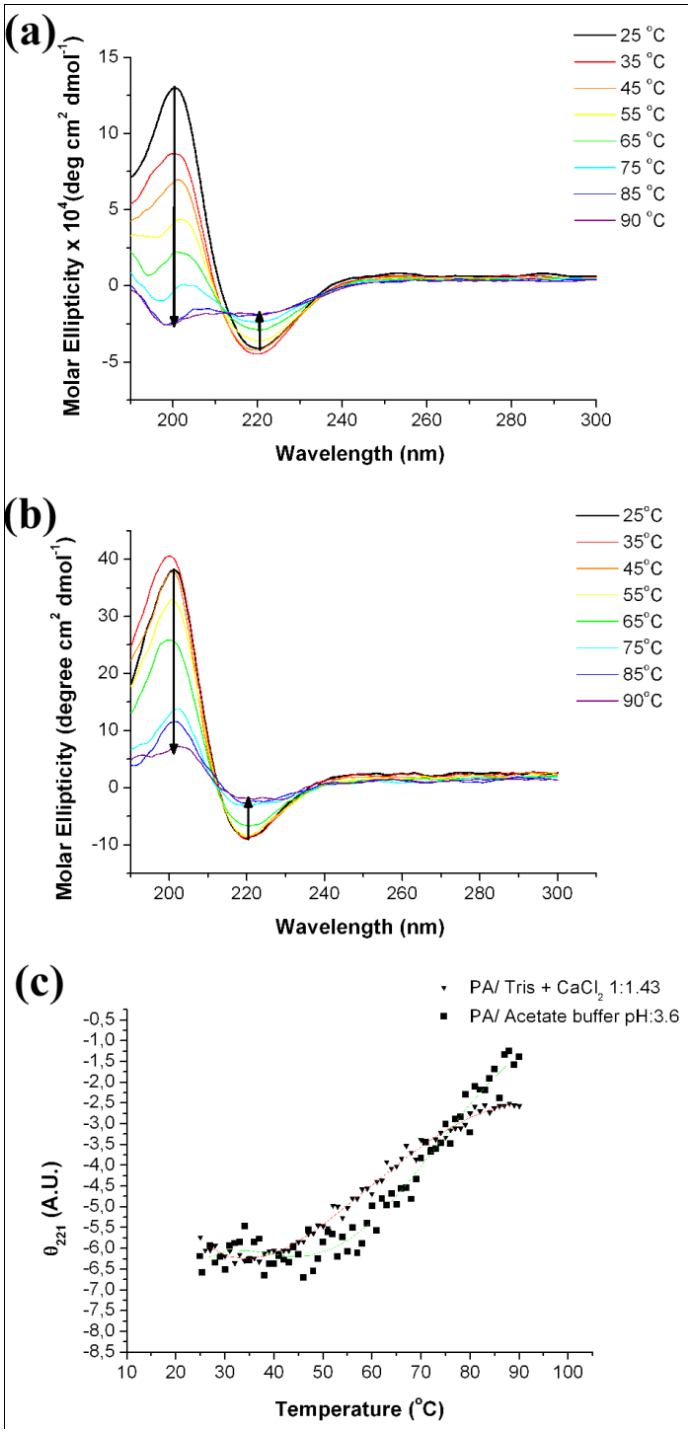

Figure 10. Circular Dichroism spectra of (a) PA with $CaCl_2$ (1:1.43 molar ratio), (b) PA with acetate buffer (pH 3.6) between 25 ºC and 90 ºC. (c) Ellipticity at 221 nm for PA with $CaCl_2$ (1:1.43 molar ratio) and PA with acetate buffer (pH 3.6) monitored between 25 ºC and 90 ºC.

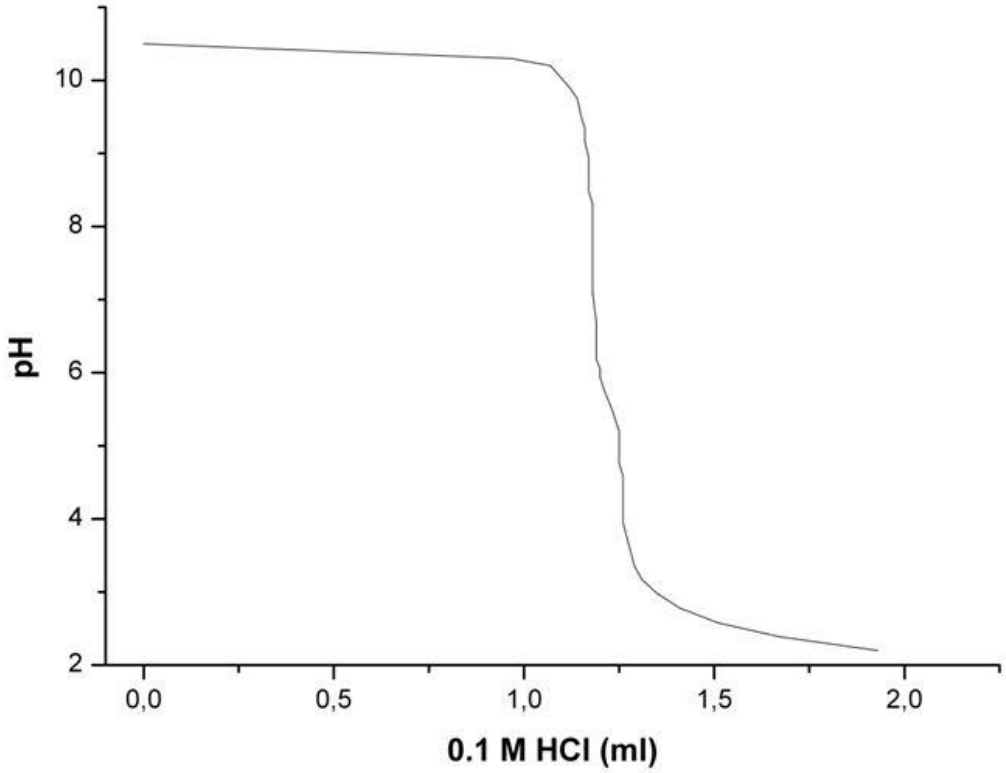

Figure 11. pH titration of the PA solution.

3.6 The mechanical Properties of Peptide Amphiphile Gels

The mechanical properties of the gels formed by PA nanofibers were studied with oscillatory rheology. Storage modulus (G') and loss modulus (G") were recorded as a function of time and temperature. The results of the time sweep rheology experiments of the PA with $CaCl_2$ and PA with HCl gels at different concentrations are shown in Figure 12. The storage moduli of the gels increased rapidly and leveled off at a plateau for each concentration because of aging process (Figure 13-20). For all concentrations, the G' value higher than G" implies that these gels act as elastic solids [31]. It is noteworthy that viscoelastic behaviors of the gels formed by HCl or $CaCl_2$ demonstrate significant differences. Storage and loss modulus values of time dependent measurements, which lasted 60 min, were compared.

The gels formed by the same PA molecules at identical concentrations with different gelators have considerable differences in stiffness due to changes in the self-assembly mechanism (Figure 12). Figure 21 shows the effect of concentration on storage moduli of the gels. (Figure 12 storage and loss modulus values were selected from time dependent measurements at time 60 min.)

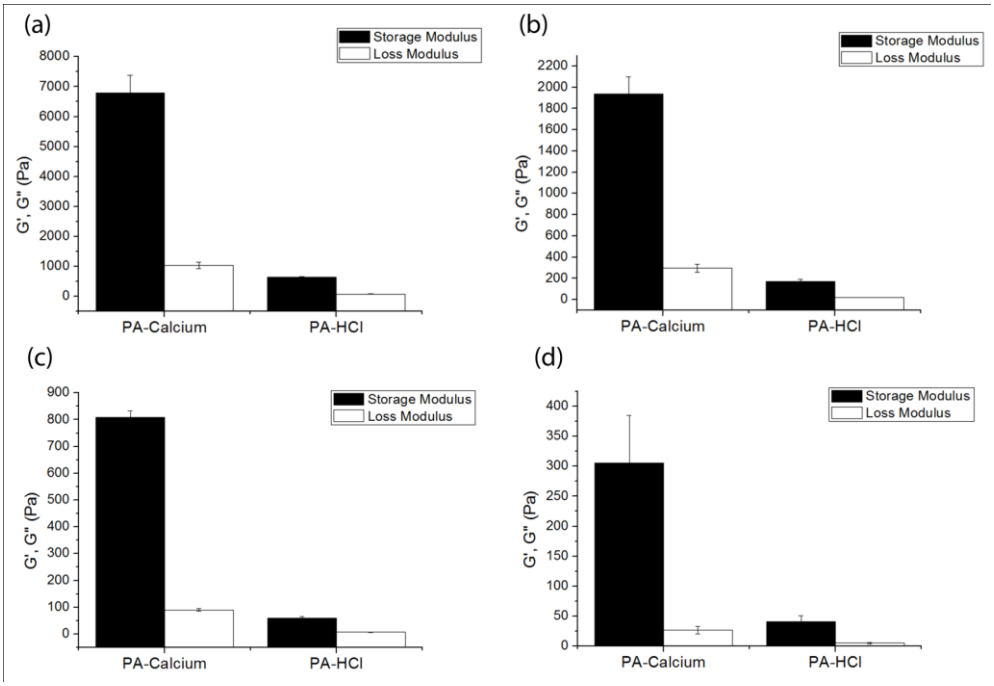

Figure 12. Time sweep oscillatory rheology measurements (t: 60 min) of PA with $CaCl_2$ and PA with HCl gels (a) 16.9 mM PA and 1.6 M HCl or $CaCl_2$, (b) 8.5 mM PA and 0.833 M HCl or $CaCl_2$, (c) 4.2 mM PA and 416.7 mM HCl or $CaCl_2$ and (d) 2.1 mM PA and 208.3 mM HCl or $CaCl_2$

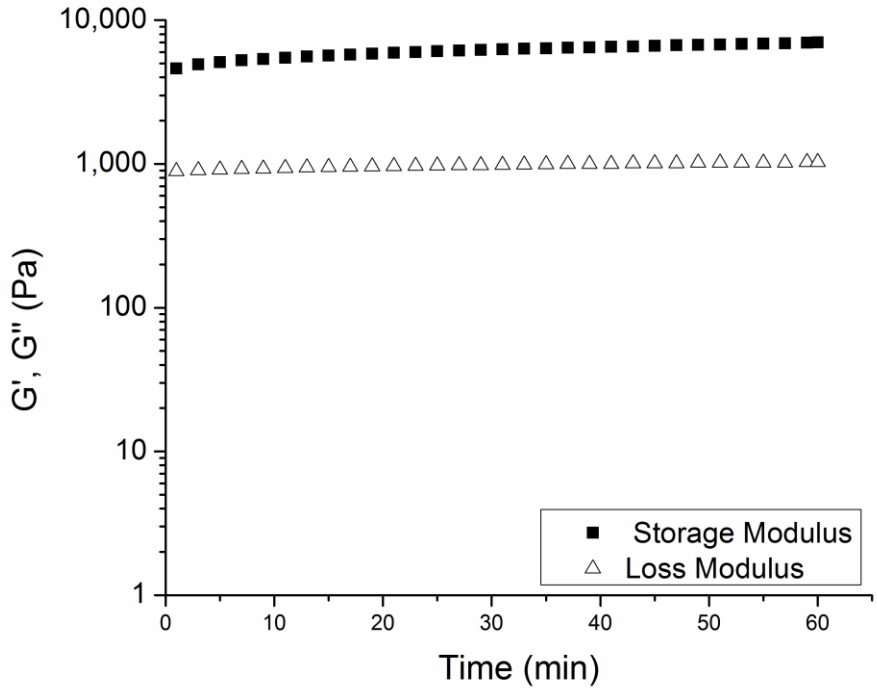

Figure 13. Time sweep oscillatory rheology measurements (t: 0-60 min) of PA with $CaCl_2$ gels. (16.9 mM PA and 1.6 M $CaCl_2$)

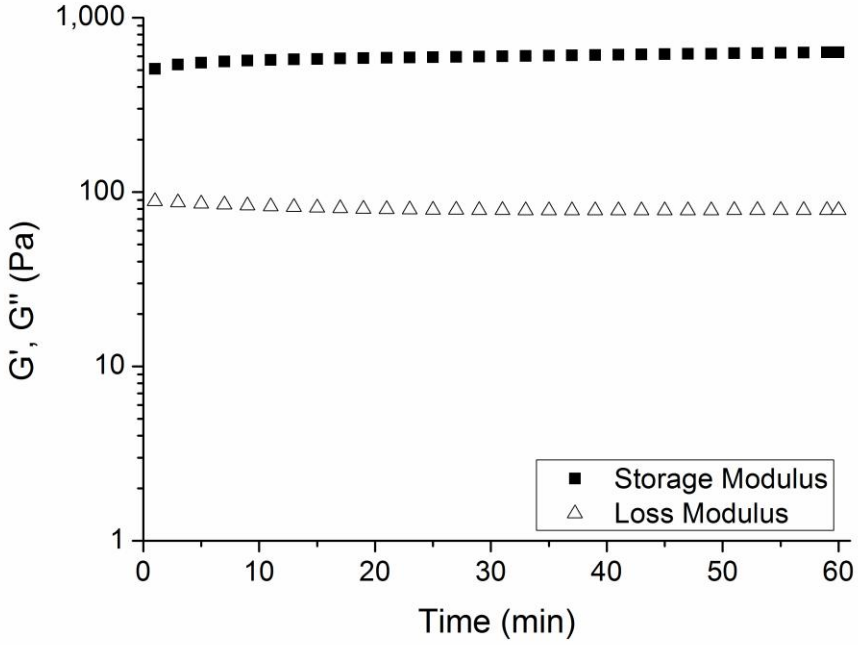

Figure 14. Time sweep oscillatory rheology measurements (t: 0-60 min) of PA with HCl gels. (16.9 mM PA and 1.6 M HCl)

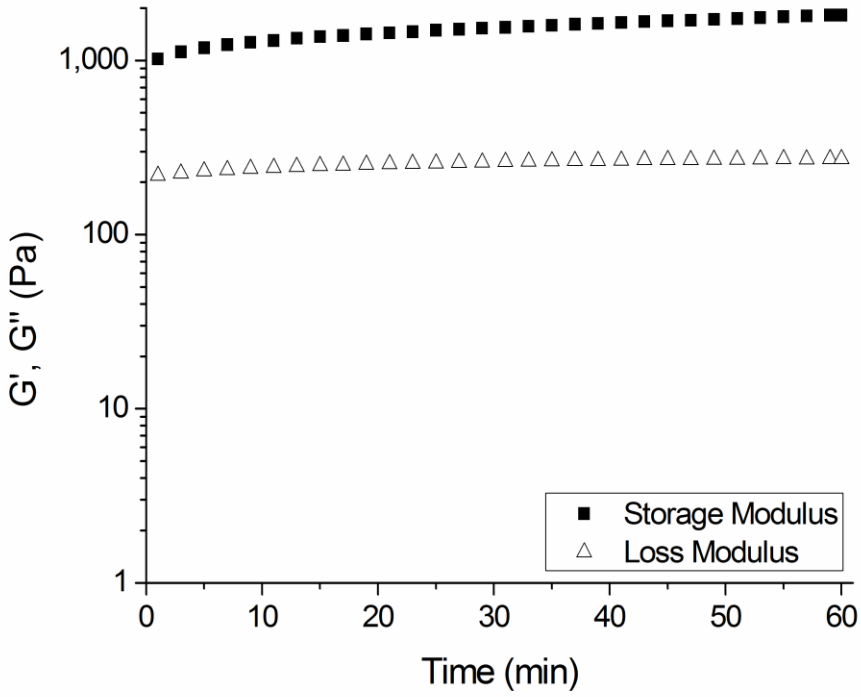

Figure 15. Time sweep oscillatory rheology measurements (t: 0-60 min) of PA with $CaCl_2$ gels. (8.5 mM PA and 0.833 M $CaCl_2$)

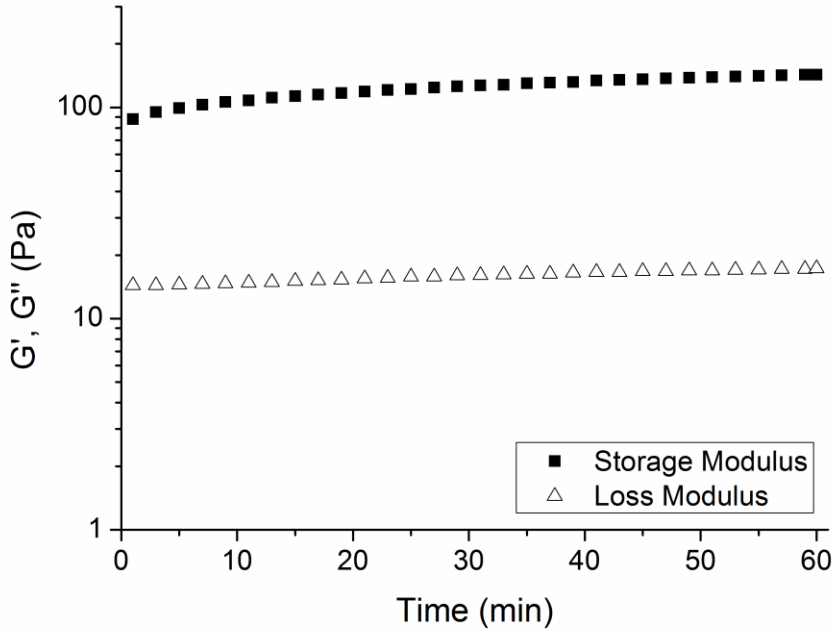

Figure 16. Time sweep oscillatory rheology measurements (t: 0-60 min) of PA with HCl gels. (8.5 mM PA and 0.833 M HCl)

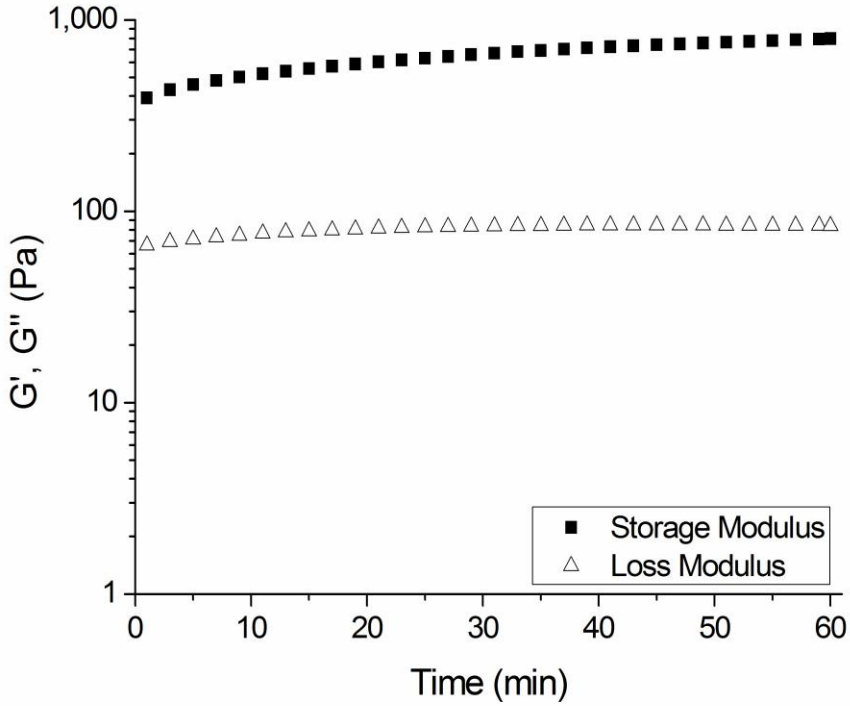

Figure 17. Time sweep oscillatory rheology measurements (t: 0-60 min) of PA with $CaCl_2$ gels. (4.2 mM PA and 416.7 mM $CaCl_2$)

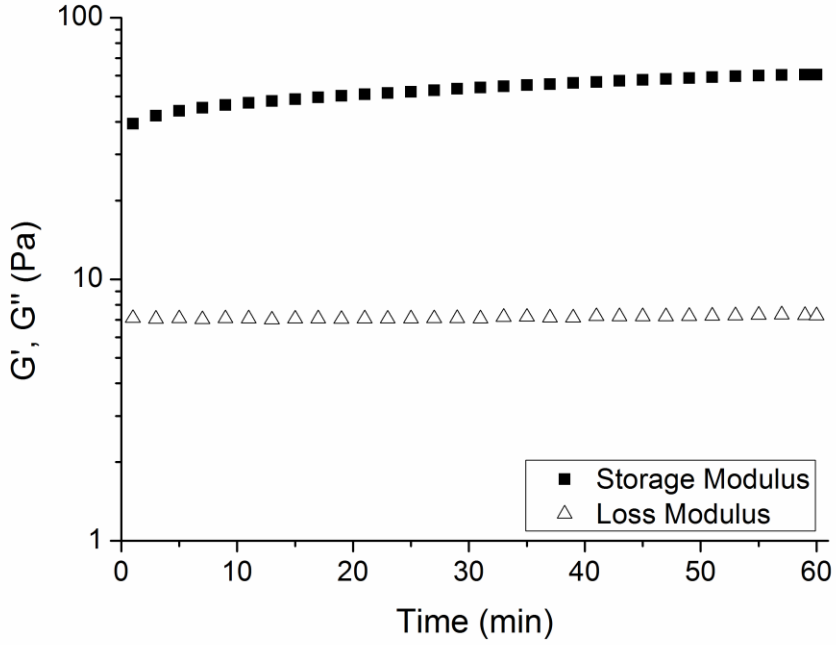

Figure 18. Time sweep oscillatory rheology measurements (t: 0-60 min) of PA with HCl gels. (4.2 mM PA and 416.7 mM HCl)

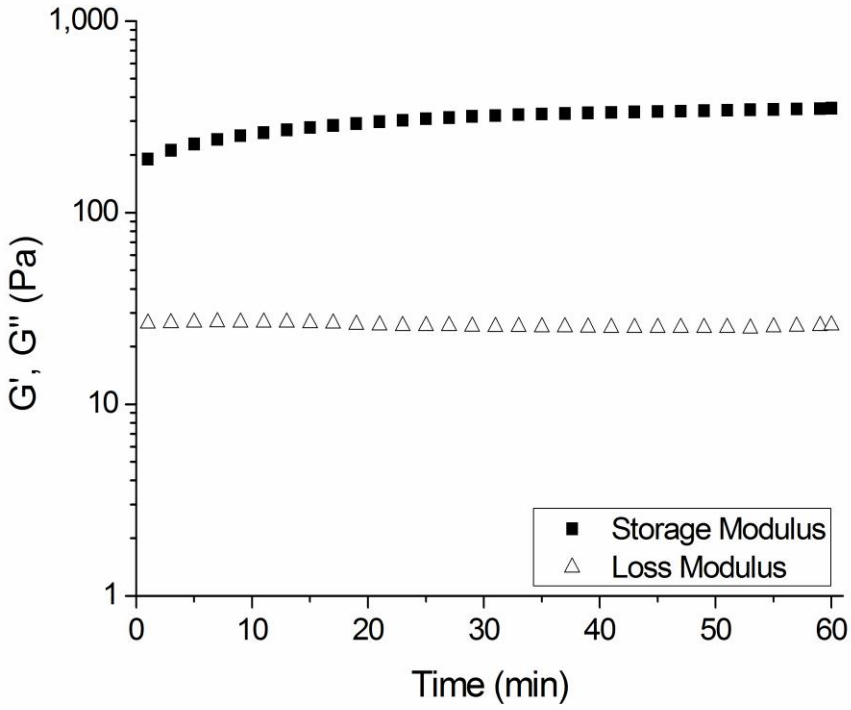

Figure 19. Time sweep oscillatory rheology measurements (t: 60 min) of PA with $CaCl_2$ gels. (2.1 mM PA and 208.3 mM $CaCl_2$)

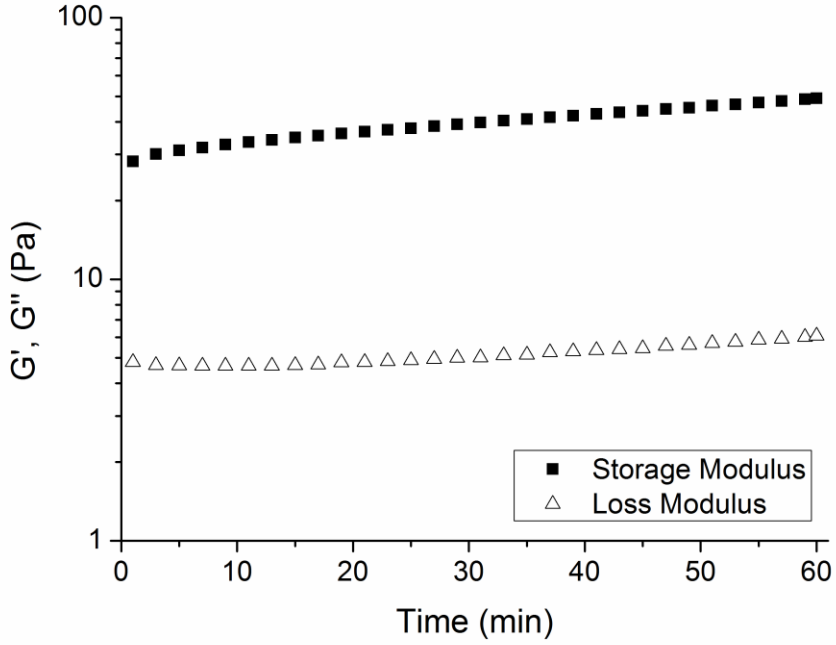

Figure 20. Time sweep oscillatory rheology measurements (t: 60 min) of PA with HCl gels. (2.1 mM PA and 208.3 mM HCl).

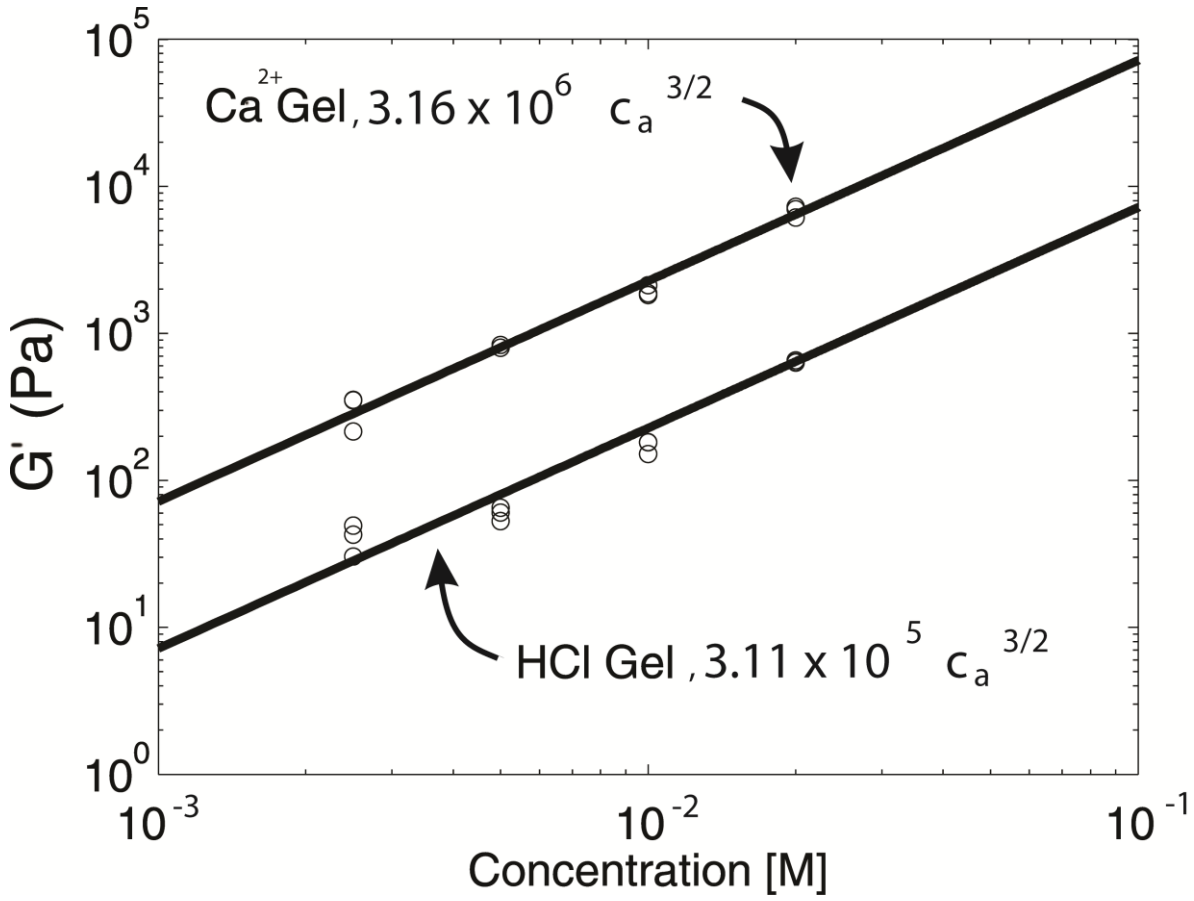

Figure 21. Macroscopic rheological study of the gels prepared with calcium and HCl shows that both gels scale with a 3/2 exponent on concentration, calcium gels being typically an order of magnitude stronger at the same concentration.

Temperature dependent oscillatory rheology was performed in order to investigate the variations in the behavior of PA gels with respect to temperature change for different gelation mechanisms (Figure 22). These PA gels respond in significantly different ways to an increase in temperature. The PA with HCl gels started to lose their mechanical properties at 30-40 °C whereas the PA with $CaCl_2$ gels started to denature at around 60-70 °C. The stability of the PA with $CaCl_2$ gels might be due to calcium bridging resulting in interfiber interactions and covering the PA fibers with calcium ions. It is widely known that metalloproteins have increased stability against temperature and this effect is observed in hot spring bacteria, proteins of which are not denatured at high temperatures [32-33]. However, the PA with HCl gels cannot withstand high temperatures. There are considerable differences for starting point and ending point values of both storage and loss moduli between time and temperature dependent experiments because of the differences in experimental set up and time interval of data points.

In the CD spectra, the denaturation profiles due to temperature increase were similar for cation triggered and pH triggered PA assemblies. However, different thermo-mechanical responses were observed for PAs gelled with $CaCl_2$ or HCl with temperature dependent oscillatory rheology. It should be noted that the gels used had concentrations at mM scale in the rheology studies whereas at the scale of 10-150 μM in the CD measurements. Thus, melting curves obtained with CD are more likely to be a reflection of the breaking of hydrogen bonds within assemblies, as a result of the nature of intrafibrillar attractions. On the

other hand, the responses observed with oscillatory rheology are related to the three-dimensional network mechanics in which interfibrillar attractions are more prominent than intrafibrillar bondings.

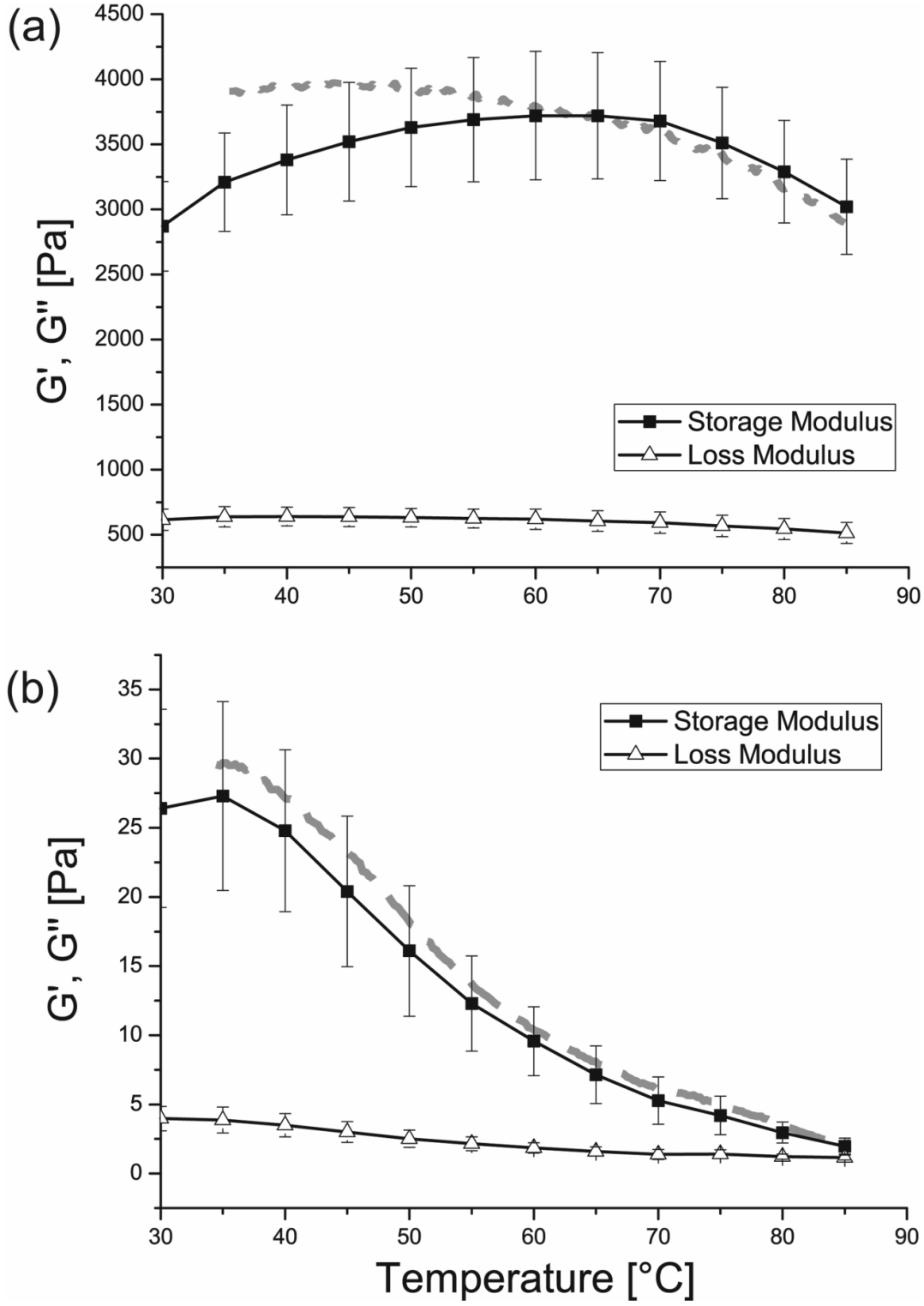

Figure 22. Temperature dependent oscillatory rheology of (a) PA with $CaCl_2$ gels (b) PA with HCl gels (Strain: 0.5%, Frequency: 10 rad/s). Dashed lines show data corrected for aging and time dependent stiffening of the gels.

Conclusion

In this chapter we studied the elasticity of supramolecular peptide amphiphile nanofiber gels. Macroscopic (rheological) measurements yielded significantly differing elastic moduli for gels prepared using calcium or HCl as the gelation agent. Circular dichroism measurements suggest that intrafiber bonds begin to disintegrate above 60 ºC for both calcium and HCl gels. However, gel elasticity displays different temperature dependence for the two different gels. These observations suggest that the model describing gel stiffness must contain effects other than those affecting single fiber elasticity. Based on these results, we point out that the discrepancy in gel stiffness for the calcium and HCl gels may arise from the difference of strength of interfiber bonds.

CHAPTER 2

Bioactive Peptide Nanofibers Promote Regeneration of Corneal Stroma

Introduction

Corneal opacification due to various reasons (trauma/diseases) resulting in vision loss, affects 10 million people in the world and it is generally treated by cornea transplantation [34-35]. However, organ donation is not favored in many cultures, the preservation of the donated tissue is problematic and the donated corneas may not be transplanted due to pathogen transmission risk and laser vision corrective surgery which makes cornea useless for transplantation. Even though, cornea is one of the easiest and highly successfully transplanted organs, it results in immunological rejection with 18% failure rate in endothelial layer breakdown cases [36]. Thus, donor shortage and the incidence of immune rejection address the need for bioengineered corneas produced with regenerative medicine approach. Additionally, for the need of cornea transplantation, the bioengineered corneas can answer the need for toxicology and drug therapy studies on cornea.

1.1 Cornea Structure

Cornea is a clear, dome shaped, highly innervated, avascular and immune privileged tissue that shields anterior part of eye from external effects [37]. Cornea is constituted of three major layers; the outermost epithelium layer, stroma and innermost endothelium layer [37-39]. Stroma is the thickest part of the cornea and formed by quiescent corneal fibroblasts -keratocytes-, which are sandwiched between collagen lamellae [40]. Bowman's membrane is positioned between epithelial layer and stroma, and Descemet's membrane separates stroma from endothelium. A healthy cornea has three priority tasks; protection of eye from the outside, being transparent for light transmission and refraction

of light for image formation. Each layer of cornea has important roles for performing these functions, which are explained in more detail below.

1.1.1 Epithelial Layer

Epithelial layer is the outermost layer of cornea that is formed by stratified, non-keratinizing squamous epithelial cells. The smooth surface of cornea has prime importance in refractive power. Tear film over epithelial layer forms a wet surface over cornea that smoothens the surface and nourishes the epithelial cells [41] . In addition to these, tear film protects the cornea by including proteolytic enzymes and lysozyme from bacteria, supplies oxygen to epithelial cells [42] and contains growth factors like EGF and supports re-epithelization of cornea [43-45]. Epithelium consists of 5-7 layers of cells and contains mainly three cell types. The surface of the epithelium is formed by squamous epithelial cells that have tight junctions between them and this layer acts as a protective barrier against foreign materials. Daughter and wing cells are positioned in the middle layer of epithelia. Bowman's membrane is an acellular layer beneath stratum germinatum and mainly consists of several types of collagen [46-47], laminin hemidesmosomes and anchoring fibrils.

The epithelial cell population in cornea is supported by stem cells that are positioned in limbal site in the eye [48]. In addition to acting as a protective barrier against foreign molecules, epithelial layer also has a role in water balance maintenance in cornea. The nerve endings in epithelium provide sensitivity to cornea. Besides these features, epithelial layer forms a smooth

surface that enables passage of oxygen and nutrients from tear and distributes to cells in cornea.

1.1.2 Stroma

Stroma is thickest part of cornea (500 μm thick), which constitutes mainly type I and V collagen fibers that are organized in parallel bundles called lamellae [49]. The uniform spacing between collagen fibers and their parallel organization in stroma are thought to role in corneal transparency and better light transmission. Each lamella is tangentially stacked to the surface of cornea and perpendicular -in terms of collagen fibril direction- to each other and contains mesenchymal-originated, quiescent fibroblast cells, –the keratocytes -, between them [40].

Keratocytes have slow turnover rate [50]. They stay in G_0 phase instead of terminally differentiating and get into two different paths in case of injury; they either enter to apoptotic or repair phases [51]. When they enter to repair phase, they either form a scar tissue in the wound area or they start to proliferate [49]. In case of cornea injury, epithelial cells secrete IL-1a which leads to cell death in upper layer of stroma [52] and induces proliferation of other keratocytes. TGF-β is known to activate myofibroblast transformation of keratocytes. [53] Secretion of TGFβ2 from epithelial cells due to loss of basement membrane causes transformation of keratocytes into myofibroblasts [54]. Myofibroblasts secrete ECM in wound area and when TGFβ2 secretion halts, they lose their myofibroblast phenotype.

ECM and stroma interaction forms the key in cell based regenerative medicine approach for corneal tissue engineering. Stroma consists of acellular extracellular matrix environment formed by parallel aligned collagen fibers, proteoglycan (PG) core proteins [55], glycosaminoglycans (GAGs) like keratin sulfate and dermatan sulfate [56] and other well known proteins, laminin and fibronectin. Lumican [57], keratocan [58-59] and mimecan [60] are the main proteoglycan core proteins and generally have attached keratin sulfate side chains. It is a known fact that the composition of ECM has a crucial role in water content [61] and collagen diameter [62-63] and arrangement [64-65] in cornea. Uniform spacing of collagen fibers have important roles in cornea's refractive power. Together with collagen arrangement, cytoplasmic crystallin proteins have important roles in transmission of light [66] and refractive index match. In addition to these, stroma is also responsible for the mechanical properties of cornea [67].

1.1.3 Endothelial Layer

Cornea endothelium is a monolayer formed by ~ 400,000 hexagonal endothelial cells that have ability of transportation. Endothelial layer has transporting activity and has an important role in cornea transparency by acting as a pump [68-69]. A fully functional endothelium pumps out water that imbibes through into stroma. If endothelium cannot perfom its function, cornea swells, loses its transparency, becomes hazy and thus loses function. Due this feature of endothelium, it has a vital position in tissue engineering of cornea.

In addition to the "pump" function of endothelium, co-culturing epithelium and endothelium has demonstrated that it affects epithelium's structure and activities [70-71]. In contradistinction to rabbit and pig endothelia, human endothelium does not proliferate *in vivo*, and culturing of these cells is rather difficult with respect to epithelial and stromal cells. Thus, cell loss in endothelial layer is compensated by spreading of the remaining cells. Although these cells are quiescent, they have not lost their replicative feature being arrested in G1 phase of cell cycle [72-73] and can be cultured on human stroma or other culturing methods [74-76].

1.2 Fully Synthetic Replacements

The synthetic replacements for cornea, known as "keratoprostheses", are artificial corneas that contain an optically clear center for functionality which is surrounded by a porous skirt that enables the attachment of the prostheses to cornea. They are mostly made of plastics and rather than aiming regeneration of cornea, they aim improvement in the function of cornea. Keratoprosthesis has been used for more than a century and there are commercially available keratoprostheses. However, the most promising keratoprostheses, which has achieved clinical success [77-78], AlphaCor^{TM} has been reported to cause progressive stroma melting and epithelial defects [79]. Although they are sufficient for visual correction of cornea and enable cornea to regain function, they are problematic in integration to host tissue and cause necrosis in eye. For this reason several researchers have tried to produce biocompatible skirts, utilizing biologically derived materials used for skirts and developed osteo-odontoprosthesis [80]. The optically clear part of the prostheses was placed

inside of a tooth; however, it had several complications like vascularization, abscess formation and extrusion. Researchers have developed other keratoprostheses with better features [81-83], however they still have limits and problems and keratoprostheses are usually suggested for patients with severe chemical burns, ocular pemphigoid, Stevens-Johnson syndrome or graft rejections [84]. For all these reasons, efficient corneal tissue engineering studies are needed for generation of healthy cornea.

1.3 Corneal Tissue Engineering Applications

Until now, many different approaches have been tried on construction of fully functional corneal equivalents; however, none has succeeded in the proper sense. These approaches has been classified under four titles as; classical tissue engineering, developmental tissue engineering, *de novo* tissue engineering and hybrid tissue engineering [85]. Classical tissue engineering aproach depends on the seeding of fibroblast cells into biodegradable matrices followed by remodelling *in vitro* or *in vivo.* Developmental tissue engineering is stimulation of fibroblast/ic cells to produce corneal stroma like structure *in vitro* prior to the implantation. *De novo* tissue engineering is the design and assembly of the ultrastructure of corneal stroma in which corneal fibroblasts can be seeded and hybrid tissue engineering approach is a combination of these methods.

Most of the tissue engineering studies aiming corneal stroma regeneration are based on the classical approach that uses a biodegradable scaffold which will enable the adhesion and proliferation of corneal cells. The main barrier for corneal tissue engineering lies in mimicking or producing the

well-organized structure of stroma. The first promising corneal tissue engineering study in which collagen based scaffolds were used, was done by Griffith et al in 1999. They have used a collagen-chondrotin sulfate substrate that is cross-linked with gluteraldehyde. Immortalized human corneal cell lines; epithelial, stromal and endothelial cells were seeded on top, middle and bottom layer of the substrate respectively and grown in cell culture media. The cultured corneal equivalents were evaluated for their transparency, histology and morphology. Engineered corneas were transparent and have responded similarly to human corneas to injuries by means of gene expression and optical clarity. Although the corneal equivalent had similar properties to human cornea, it was not sufficient for cornea replacement.

The mechanical properties of stroma and stroma analog "scaffolds" are vital for tissue engineering of cornea. Synthetic polymer-collagen scaffolds have been used in an effort to increase mechanical strength of scaffolds. The synthetic material is expected to deal with mechanical requirements that provide mechanical sufficiency and collagen part provides biocompatibility and biofunctionality to the scaffold. For this purpose, in 2003, Li et al used a collagen-copolymer scaffold, in which copolymer enables proteins and peptides to cross-link. In this study, YIGSR peptide sequence was used for providing bioactivity. YIGSR is a motif of laminin responsible for adhesion and has been proven to improve epithelial cell growth [86] and neurite extension [87]. Although these scaffolds were reported to be weaker than human cornea, they were strong enough for surgical procedures like suturing [88]. The nerve re-growth and touch sensitivity has been reported to occur in a relatively shorter

time in cornea grafts with the composite material than the allografts. This study demonstrated the importance of utilizing scaffolds that contain different materials having distinct properties together with co-usage of synthetic polymers and natural materials like collagen.

1.4 Corneal Tissue Engineering with Peptide Amphiphiles

Peptide amphiphiles (PA) are self-assembling molecules that are composed of a hydrophobic alkyl tail and a peptide segment. PA molecules tend to self assemble into nanofibers through intermolecular hydrogen bonding [1]. The interactions between these nanofibers induce formation of a three dimensional network that encapsulates water in aqueous environment forming gels, which can mimic extracellular matrix. PA based nanofiber networks are promising biomaterials for tissue engineering applications due to their flexibility in terms of physical, chemical and biological features. Bioactive PA gels have been used for a number of different applications like cartilage [89], bone [90], neural regeneration [13] and angiogenesis [91] as a synthetic extracellular matrix mimicking agent.

In this study, we utilized PA molecules in order to increase stroma thickness through tissue regeneration. The PA molecules were designed to have a hydrophobic alkyl chain and a β-sheet forming amino acid sequence, both of which were used to induce nanofiber formation through self-assembly, and a bioactive peptide sequence that contained laminin derived [86, 92] “YIGSR” peptide sequence which is known to play a role in cell adhesion [93] and migration [94]. The chemical and physical characterization of PA gelswere

investigated with rheology, circular dichroism, scanning electron microscopy, transmission electron microscopy and atomic force microscopy. The biocompatibility and bioactivity of PA hydrogels were tested on human corneal fibroblast (HTK) cells.

Materials and Methods

2.1 General Methods

The identity and purity of the PAs were assessed by LC-MS (Agilent 1200/6530) equipped with either Agilent Zorbax Extend-C18 2.1 x 50 mm column for basic conditions or Zorbax SB-C8 4.6 mm x 100 mm column for acidic conditions. Agilent preparative reverse-phase HPLC system equipped with Zorbax Extend-C18 21.2 x 150 mm column was used for basic conditions and Zorbax SB-C8 21.2 × 150 mm column was used for acidic conditions for the purification of peptides. A gradient of (a) water (0.1% formic acid (for acidic conditions) or 0.1% NH_4OH (for basic conditions)) and (b) acetonitrile (0.1% formic acid (for acidic conditions) or 0.1% NH_4OH (for basic conditions)) was used.

2.2 Materials

9-Fluorenylmethoxycarbonyl (Fmoc) protected amino acids, lauric acid, [4-[α-(2',4'-dimethoxyphenyl) Fmoc-amino methyl] phenoxy] acetomidonorleucyl- MBHA resin (Rink amide MBHA resin), 2-(1H-Benzotriazol-1-yl)-1,1,3,3-tetramethyluronium hexafluorophosphate (HBTU), and diisopropylethylamine (DIEA) were purchased from Merck and ABCR. 100-200 mesh Wang resin was purchased from NovaBiochem and valine was loaded onto it for Fmoc-Val-Wang resin. All other chemicals and materials used in this study were analytical grade and obtained from Invitrogen, Fisher, Merck, Alfa Aesar, and Sigma-Aldrich.

2.3 Synthesis and Purification of Peptide Amphiphile Molecules

Peptide amphiphile (PA) molecules were synthesized by using fluorenylmethoxycarbonyl (Fmoc) chemistry. Synthesis was performed manually on a 1 mmole scale using a 50 ml peptide synthesis vessel on a wrist action shaker. Either Fmoc-Glu-(OtBu)-Wang resin or Rink amide MBHA resin was used for peptide synthesis. For each coupling reaction, Fmoc groups were removed by shaking resins in 20% piperidine in N,N-dimethylformamide (DMF) for 20 min. After each reaction, resins were washed three times with DMF, dichloromethane (DCM) and DMF respectively. All amino acids were activated by adding 2 molar equivalents of amino acid to 1.95 equivalents of O-Benzotriazole-N,N,N',N'-tetramethyl-uronium-hexafluoro-phosphate (HBTU) and dissolved in 10 ml of DMF. After complete dissolution of amino acid and HBTU in DMF, 3 molar equivalents of N-ethyl-diisopropylamine (DIEA) were added into the solution. The solution was mixed thoroughly and kept for 3 min before adding to the resin. Each coupling reaction was performed for 2.5 h. Lauric acid was coupled to the peptide's N-terminal. Ninhydrin test was performed after addition of each amino acid and after addition of the lauric acid. When ninhydrin test yielded positive results, coupling reaction was repeated; otherwise 10 ml of 10% acetic anhydride in DMF was added and resins were shaken for 30 min. Peptide cleavage and removal of the protecting groups were performed with 95:2.5:2.5 trifluoroacetic acid (TFA): triisopropylsilane (TIS): water for 2.5 h at room temperature. After cleavage reaction, PA molecules were collected in a clean round bottom flask and DCM wash was performed for several times. Collected solution was rotary-evaporated. After evaporation, ice-

cold diethyl ether was added and was left at -20 °C overnight. PA-diethyl ether mixture was collected in 50 ml falcon tubes and centrifuged at 8000 rpm for 25 min. Supernatant was decanted and the remaining diethyl ether was evaporated. The pellet was dissolved in deionized H_2O at a resistance of 18.2 Ω and was freeze-dried.

2.4 Oscillatory Rheology

Rheology measurements were performed with an Anton Paar Physica RM301 Rheometer operating with a 25 mm parallel plate at a 0.5 mm gap distance. Freeze-dried YIGSR-PA molecules and CS were dissolved in 270 mM isotonic sucrose solution and the pH was adjusted to ~7 with 0.1 M NaOH solution for the in vivo experiment model. 200 µl of 2.5 (w/v) % YIGSR-PA was mixed with 50 µl of 3 (w/v) % CS. For the in vitro experiment model, lyophilized YIGSR-PA, Lys-PA and Glu-PA molecules were dissolved in deionized water and pH was adjusted to ~7 with 0.1 M NaOH solution. 166 µl of 2 wt % YIGSR-PA was mixed with 84 µl of 2 wt % Glu-PA. 166 µl of 2 wt % Lys-PA was mixed with 84 µl of 2 wt % Glu-PA. The gel was prepared on the lower plate of the rheometer and gelling agents were added dropwise in order to prevent any deformation of the gel structure. The stage temperature was adjusted to 25 °C and all samples were allowed to equilibrate for 15 min to achieve stable gel formation before the measurements were taken. Wet tissue paper was placed inside the chamber around the edge of the plate to provide a humid environment and prevent solvent evaporation from the sample during the experiments. Measurements were taken for 60 min at 10 rad/s and 0.5% strain.

2.5 Circular Dichroism (CD)

CD spectra of the PA solutions were obtained using a J-815 Jasco spectrophotometer in the far UV region using quartz cuvettes with 1 mm path length. The spectra were acquired for three formulations; YIGSR-PA at pH 7, YIGSR-PA mixed with CS and YIGSR-PA mixed with Glu-PA. PA molecules (YIGSR-PA, and Glu-PA) and CS were dissolved in deionized water at 0.01 wt % and 0.012 wt % respectively. pH of each solution was adjusted to 7 before use. YIGSR-PA/Glu-PA solution was mixed at 2:1 volume ratio and YIGSR-PA/CS solutions were mixed at 4:1 volume ratio. Averages of three scans of each sample were taken. CD spectra were obtained from 190 nm to 300 nm at a digital integration time of 1 s, a band width of 1 nm and a data pitch of 0.1 nm.

2.6 Scanning Electron Microscopy (SEM)

The nanofiber network formation ability of YIGSR-PA at different conditions was observed with scanning electron microscopy (SEM). 2.5 wt % YIGSR-PA solution was prepared in isotonic sucrose solution (270 mM). In order to form YIGSR-PA/CS gel, 20 μL of PA solution was mixed with 5 μL of aqueous 3 wt % CS (Sigma- Aldrich C6737) solution. For YIGSR-PA/E-PA gels, 20 μL of 2.5 wt % YIGSR-PA solution was mixed with 10 μL of 2.5 wt % E-OH PA. For Lys-PA/E-PA gels, 20 μL of 2.5 wt % Lys-PA solution was mixed with 10 μL of 2.5 wt % E-OH PA. The mixing ratio was adjusted to screen the charges on the positively charged YIGSR-PA molecules at phsiological conditions. Gels were incubated for 10 min for maturation and dehydrated gradually with increasing concentrations of ethanol. Ethanol was then removed by critical point drying (Tousimis, Autosamdri-815B). The

samples were sputter-coated twice with 3 nm of Au/Pd to ensure complete coating. Visualization of the nanofiber networks was carried out with an FEI Quanta 200 FEG scanning electron microscope with ETD detector with high vacuum between 10-30 kV and an average working distance of 10 mm.

2.7 Atomic Force Microscopy (AFM)

AFM samples were prepared on 1 cm^2 silicon wafers (with low residual roughness (<1 $nm/\mu m^2$)) using 30 µl of 0.01 wt % PA solutions. 40 µl of 0.01 wt % YIGSR-PA was mixed with 10 µl of 0.012 wt % chondroitin sulfate. 65 µl of 0.01 wt % YIGSR-PA was mixed with 35 µl of 0.01 wt % Glu-PA. 30 µl of 0.01 wt % Lys-PA was mixed with 15 µl of 0.01 wt % Glu-PA. Samples were drop casted on silicon wafers and left for air drying in a chemical fume hood. Dynamic mode imaging was used to image the topography of the resulting samples, using appropriate cantilevers (cantilever stiffness of k=3-40 N/m, resonance frequency of f_0=70-350 KHz for the dynamic mode).

2.8 Cell Culture and Maintenance

The viability, adhesion and proliferation profiles of cells on YIGSR-PA nanofibers were studied using human corneal keratocytes (HTKs) previously developed by Jester et al. [95]. HTKs were cultured in 75 cm^2 polystyrene cell culture flasks with Dulbecco's modified eagle serum (DMEM) containing 10% Fetal Bovine Serum (FBS) and 1% Penicillin/Streptomycin. HTKs are known to express myofibroblast markers in media with 10% FBS and keratocyte markers in serum free media [95]. In case of corneal wounding, keratocytes differentiate into myofibroblasts. In order to simulate the environment of the in vivo

experiment, where corneas were wounded by opening corneal pockets, HTKs were cultured at 10% FBS. All of the in vitro experiments and passaging of cells were performed when cells became ~80% confluent. Cells were diluted 1:3 for splitting.

2.9 In vitro Application of Peptide Amphiphile Molecules

Three experimental groups have been designed to assess the biocompatibility and bioactivity of YIGSR-PA on HTK cells; a) collagen, the main component of ECM was used as a positive control, b) YIGSR-PA was mixed with Glu-PA (Figure 1) and c) non-coated tissue culture plate was used as negative control. For each experiment, 0.2 wt % YIGSR-PA and Glu-PA was mixed with 1.85:1 volume ratio and 0.01 wt % collagen solution was used. Experiments were performed in 96-well plates containing 100 µl of total PA solution and 35 µl collagen solution. For 24-well plates, 600 µl of total PA solution and 210 µl collagen solution were used. Coated plates were incubated at 37 °C for 45 min and water evaporated within laminar flow hood overnight. After complete drying of collagen and PA coated wells, plates were UV-sterilized before culturing HTKs. 2×10^4 and 3×10^3 HTKs were seeded into each well of 24-well plates and 96-well plates, respectively. PA and collagen coatings were performed on glass coverslips placed within wells of 24-well plates.

2.10 Biocompatibility assesment by using viability assays

Live/Dead Assay was used for determination of the effect of YIGSR-PA on viability of HTKs. 3×10^3 cells were seeded in each well (n=5) of 96-well

plates and cultured for 3 days. At the end of incubation time, medium was aspirated and cells were washed with PBS, and stained with 100 µL of 2 µM Calcein AM and 4 µM ethidium homodimer-1 solution. After 45 min of incubation at room temperature, the quantification of cytotoxicity was determined by calculating the ratio of live cells to total cells by using a flourescence microscope.

2.11 Cell adhesion assays for cell-material interaction analysis

Adhesion of HTKs seeded on PA coated, collagen coated and bare glass was assessed by staining filamentous actins and nuclei with TRITC-conjugated phalloidin and TO-PRO®-3 iodide, respectively. After preparation of PA and collagen coated wells within 24-well plates, 2 x 10^4 HTKs were seeded in each well and incubated for 24 h. At the end of incubation time, cells were fixed with 4% paraformaldehyde and permeabilized with 0.1% Triton-X 100. Following PBS wash, TRITC-conjugated phalloidin staining and TO-PRO®-3 iodide staining were performed. Cells were kept in PBS for 45-60 min before observation under Zeiss LSM 510 confocal microscope.

The HTK and surface interaction at micro scale was assessed by electron microscopy. HTKs cultured on PA or collagen coated and bare glass surfaces were incubated for 24 h. 2.5% gluteraldehyde fixation was followed by 1% OsO_4 fixation after which water content was removed by incubation in gradual increases of ethanol. Samples within 100% ethanol were critical point dried with Tourismis Autosamdri®-815B critical-point-drier. Dried samples were coated

with 4 nm Au/Pd and observed under high vacuum mode with FEI Quanta 200 FEG scanning electron microscope equipped with ETD detector.

2.12 Cell proliferation assays

The proliferation capacity of corneal fibroblasts was assessed with 5-bromodeoxyuridine (BrdU) incorporation. Corneal fibroblasts were cultured in 96-well plates (n=5) on uncoated, YIGSR-PA coated and collagen coated surfaces for 72 hr. At 54 hr, BrdU labelling solution was added to cells at a final concentration of 10 μM and incubated for 18 hr. Cell culture medium was tapped off and 200 μl/well of FixDenat solution was added and cells were incubated for another 30 min at RT. Fix/Denat solution was tapped off and 100 μl/well of anti-BrdU-POD working solution was added and incubated for 90 min. Supernatant was removed by tapping off and cells were washed with PBS for three times. Cells were dried with tapping the plate and 100 μl/well substrate solution was added. Cells were incubated for 30 min at RT with substrate solution and the absorbance was measured every 5 min at 370 nm with SpectraMax M5 Microplate Reader, Molecular Devices. Results obtained at 15^{th} min were used for the analysis.

Results and Discussion

3.1 Experimental Conditions

Physical and chemical characterization of YIGSR-PA molecules were performed for two different conditions. The differences between these conditions originated due to application conditions of YIGSR-PA molecules for *in vitro* and *in vivo* experiments.

The first condition was to mimic the gels used for *in vivo* experiments. During the *in vivo* experiments, YIGSR-PA was injected into corneal pockets which were surgically opened within stroma. Although YIGSR-PA was injected in solution form, the solution transformed into hydrogels at the injection site since stroma is rich in negatively charged glycosaminoglycans (GAG), which induce nanofiber formation with these positively charged PA molecules through charge neutralization. Chondroitin sulfate (CS) was used as a model GAG for this purpose, since it is a prevalent GAG within corneal stroma.

Second condition was utilized to mimic the environment of *in vitro* experiments, where negatively charged Glu-PA was used as a non-bioactive gelator of positively charged YIGSR-PA through self-assembly of the nanofibers caused by charge neutralization.

3.2 Design, Synthesis and Purification of Peptide Amphiphiles

Lauryl-VVAGKYIGSR-Am (YIGSR-PA), lauryl-VVAGE (Glu-PA) and lauryl-VVAGK-Am (Lys-PA) molecules were designed and synthesized to form nanofibers as artificial ECM material (Figure 23). YIGSR-PA contains “YIGSR” epitope of laminin and is known for its activity on cell adhesion [93]

and migration [94]. “YIGSR” epitope has been used for a number of cell types like corneal epithelial cells [96], fibroblast cells [97] and neonatal cardiac myocytes [98]. In this study, YIGSR signal was used for inducing corneal fibroblast migration and adhesion. Glu-PA is a negatively charged PA molecule at physiological pH and was used as a gelation agent for YIGSR-PA. For *in vitro* studies, YIGSR-PA was mixed with Glu-PA, which does not contain a bioactive epitope, in order to observe the bioactivity of “YIGSR” epitope only. Lys-PA is a positively charged PA molecule at pH 7.4 and was used as a control to test the bioactivity of the YIGSR-PA. The PA molecules were synthesized and purified (Figure 23-29) with Agilent 6530-1200 Q-TOF LC/MS equipped with ESI-MS and a Zorbax Extend C18 column for basic conditions and Zorbax SB-C8 21.2 × 150 mm column was used for acidic conditions.

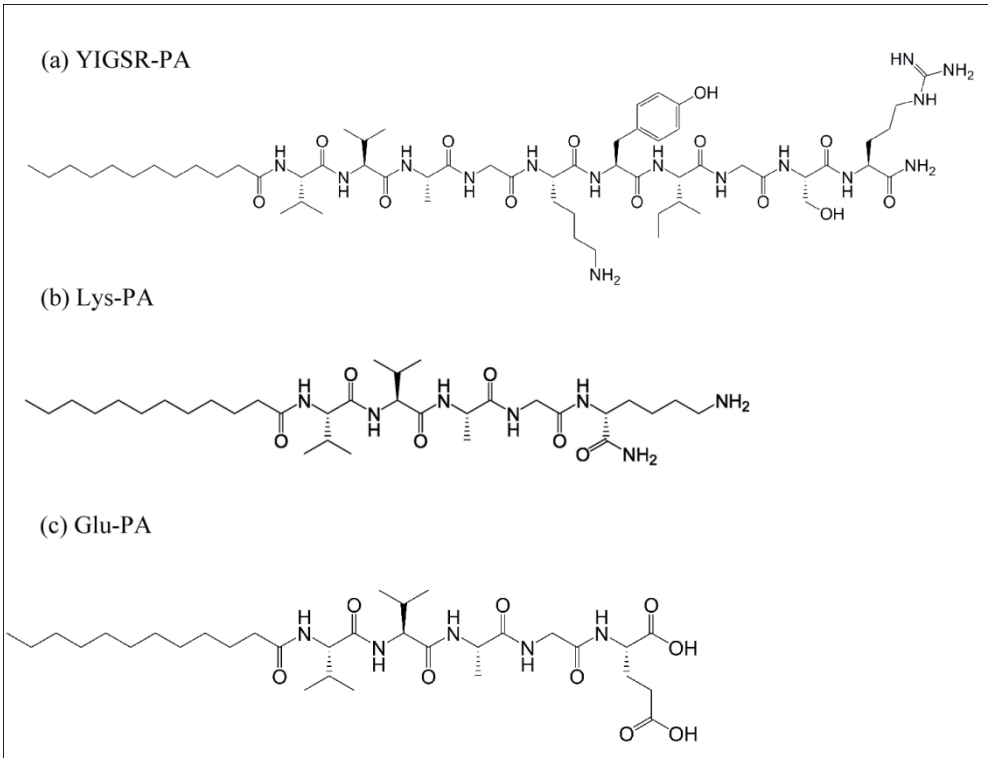

Figure 23. Chemical structure of the (a) YIGSR-PA, (b) Lys-PA and (c) Glu-PA.

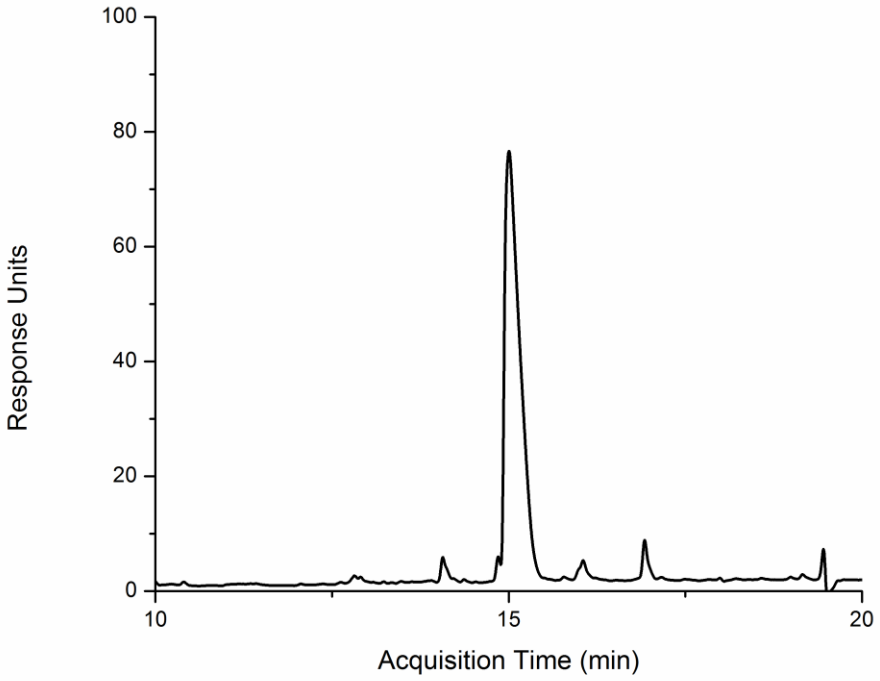

Figure 24. RP-HPLC chromatogram of the YIGSR-PA. Absorbance at 220 nm vs retention time graph.

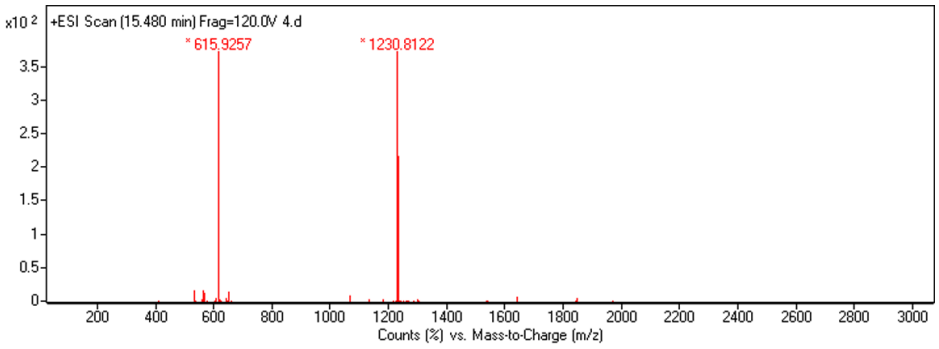

Figure 25. Electrospray ionization mass spectra of the YIGSR-PA. $(M+H)_{observed}$+=1230.81, $(M+H)_{calculated}$+=1230.81, $(M+2H)+2/2_{observed}$+= 615.92 , $(M+2H)+2/2_{calculated}$+= 615.92.

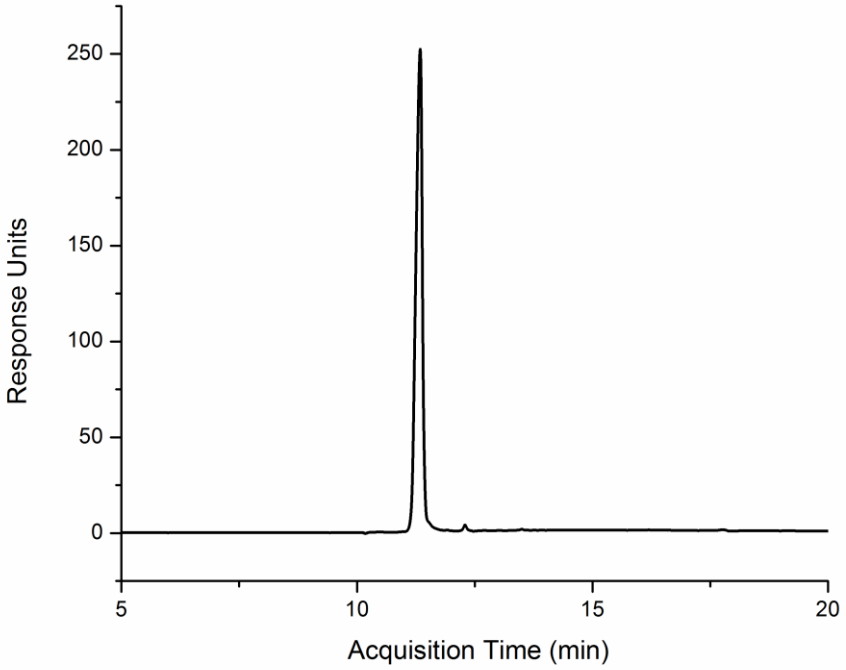

Figure 26. RP-HPLC chromatogram of the Glu-PA. Absorbance at 220 nm vs retention time graph.

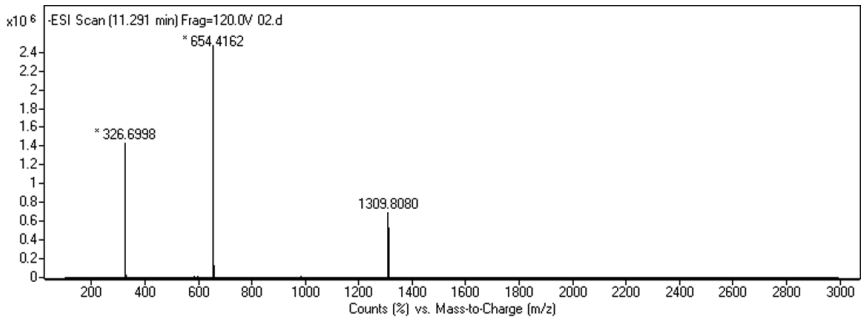

Figure 27. Electrospray ionization mass spectra of the Glu-PA. $(M-H)^{-1}_{observed}$+=654.41, $(M-H)^{-1}_{calculated}$+= 654.41, $(M-2H)/2^{-2}_{observed}$+= 326.69, $(M-2H)/2^{-2}_{calculated}$+= 326.69, $(2M-H)^{-1}_{observed}$+= 1309.80, $(2M-H)^{-1}_{calculated}$+= 1309.80.

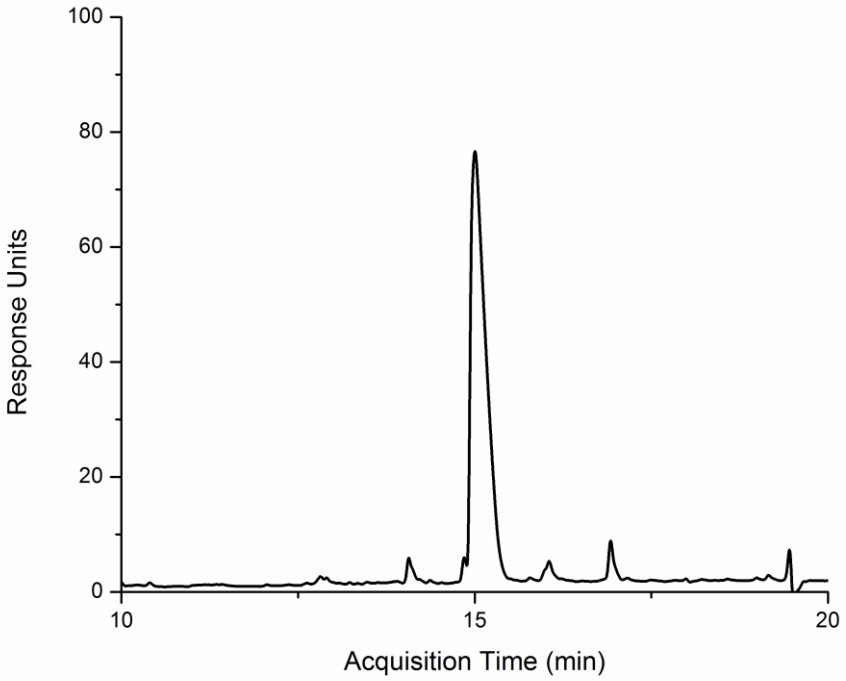

Figure 28. RP-HPLC chromatogram of the Lys-PA. Absorbance at 220 nm vs retention time graph.

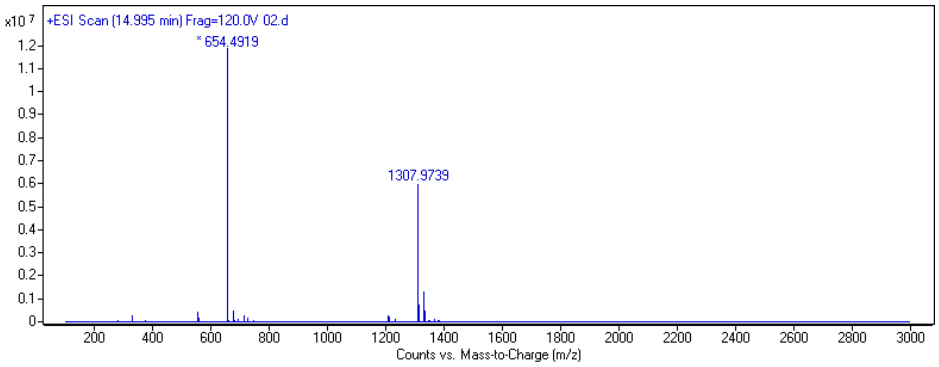

Figure 29. Electrospray ionization mass spectra of the Lys-PA. $(M+H)_{observed}^{+}$=654.49, $(M+H)_{calculated}^{+}$=654.49,$(2M+H)_{observed+=}$ 1307,97 , $(2M+H)_{calculated+=}$ 1307,97.

3.3 Nanoscale Morphology of Peptide Amphiphile Molecules

3.3.1 SEM Imaging of Peptide Amphiphile Nanofiber Networks

Morphology of the network formed by PA nanofibers was studied with SEM. The nanofiber formation of YIGSR-PA molecules through addition of chondroitin sulfate or negatively charged non-bioactive Glu-PA and Lys-PA molecules with Glu-PA are shown in Figure 30 a, b and c, respectively. PA nanofibers formed an ECM like nanofibrous network.

3.3.2 AFM Imaging of Peptide Amphiphile Nanofibers

PA nanofiber formation through addition of chondroitin sulfate or Glu-PA to YIGSR-PA and Lys-PA through addition of Glu-PA was also studied with AFM (Figure 30 d, e and f, respectively). AFM results indicated that PA molecules formed nanofibers in several lengths for different combinations. For all three conditions, PA molecules formed similar nanofiber networks observed with SEM. On the other hand, there is a significant difference between Glu-PA and chondroitin sulfate directed PA nanofiber formation observed with AFM. The difference is due to the drying of samples during AFM sample preparation that leads to fiber bundle formation. The bundling capacity of PA nanofibers depends on the self-assembly/cross-link mechanism affecting the nanofiber formation process, and is further explained in detail at Ref [99].

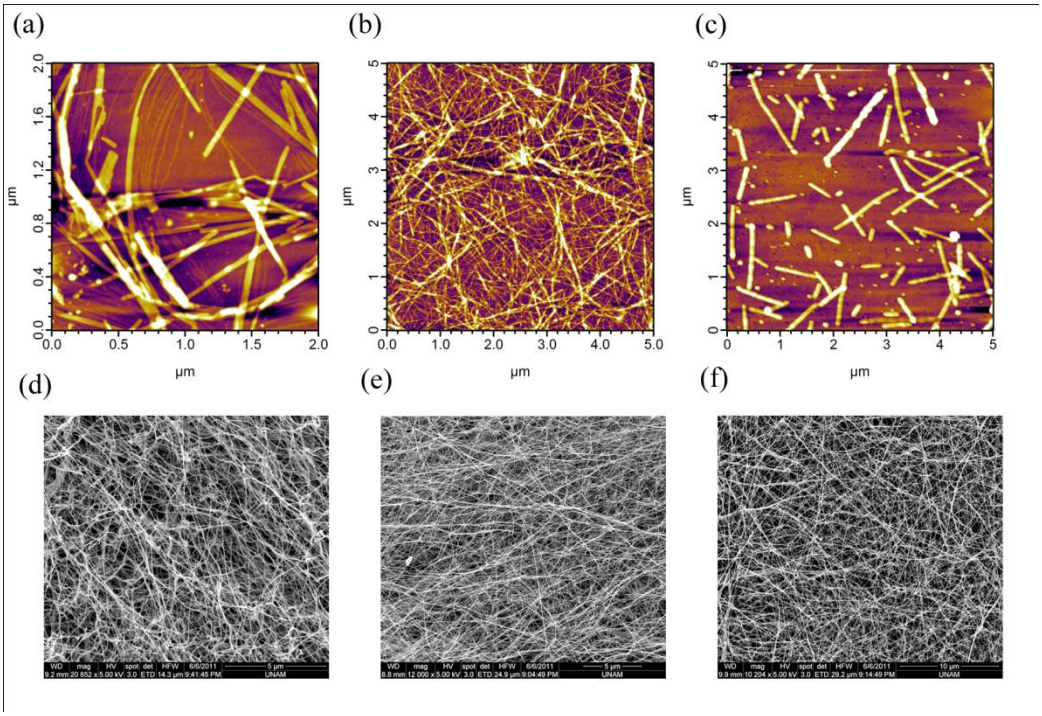

Figure 30. Scanning electron micrographs of (a) Lys-PA gel formed with Glu-PA, (b) YIGSR-PA gel formed with Glu-PA and (c)YIGSR-PA gel formed with chondroitin sulfate (scale bars are 5 µm for a and b, 10 µm for c). AFM topography images of (d) Lys-PA gel formed with Glu-PA, (e) Lys-PA gel formed with Glu-PA and (f) YIGSR-PA gel formed with chondroitin sulfate.

3.4 Circular Dichroism Spectra of Peptide Amphiphile Molecules

Circular dichroism spectra were used to study the secondary structure of PA nanofibers. The signature of β-sheets observed in the CD spectra display a negative band at 220 nm and a positive band at 195 nm. The β-sheet secondary structure was prevalent for YIGSR-PA and Glu-PA at physiological pH. The observation of β-sheet secondary structure indicates formation of hydrogen bonding networks which in turn leads to formation of nanostructures with the help of hydrophobic collapse of alkyl groups, thus supports the viscous behavior of both PAs at pH 7.4 (Figure 31).

3.5 Analysis of Mechanical Properties of PA Gels with Oscilatory Rheology

The mechanical properties of PA matrices were studied with oscillatory rheology because mechanical properties of extracellular environment have crucial roles in vital functions of cells. The measurements (G’ and G’’) were recorded as a function of time. The storage modulus for both PA gels was higher than the loss modulus, which implies the viscoelastic nature of PA gels (Figure 32). The storage and loss moduli of the PA gels were increased rapidly and leveled off for each condition due to the aging process.

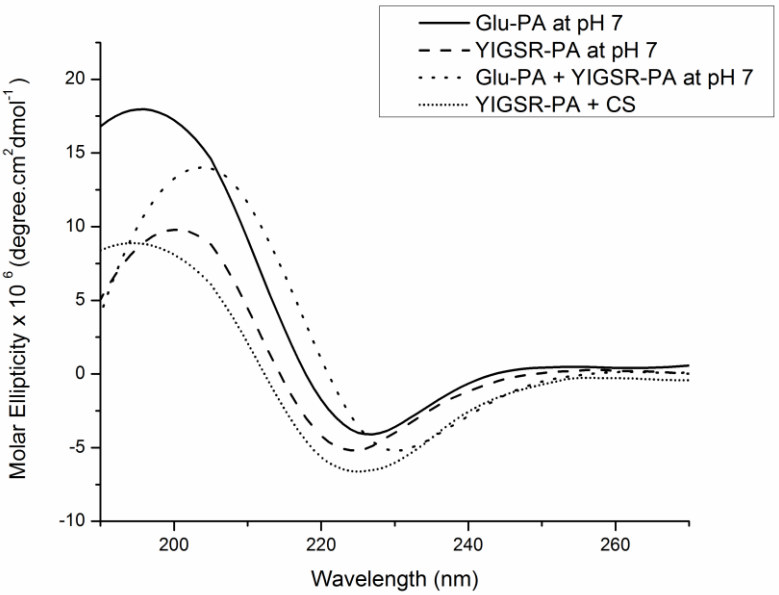

Figure 31. Circular dichroism spectra of the YIGSR-PA and Glu-PA at different conditions.

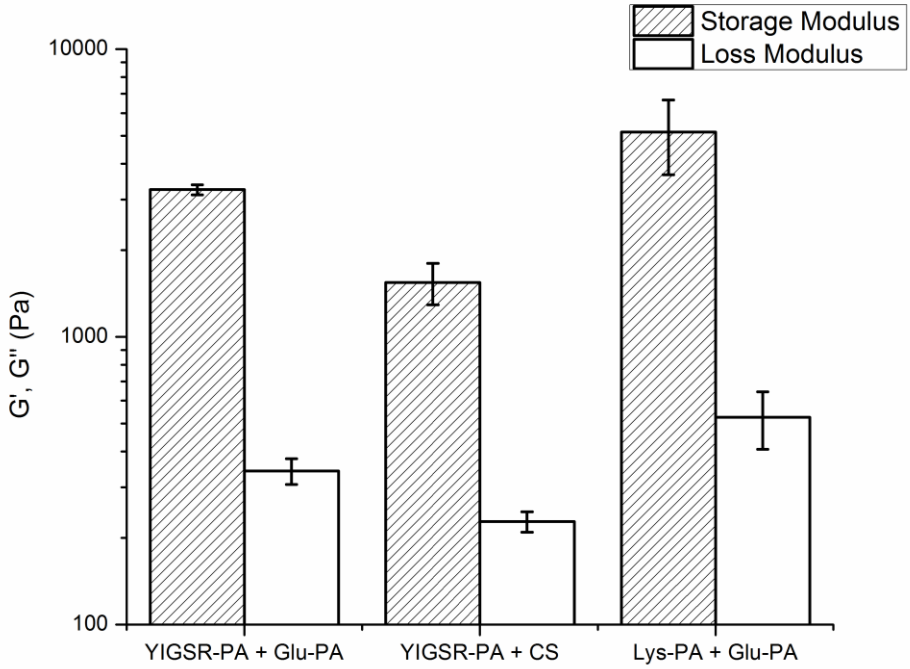

Figure 32. Time sweep oscillatory rheology measurements (t: 60 min) of YIGSR-PA with Glu-PA, YIGSR-PA with chondroitin sulfate and Lys-PA with Glu-PA gels.

3.6 Cell Culture Applications of Peptide Amphiphile Molecules

3.6.1 Cell Viability Measurements

Biocompatibility of YIGSR-PA molecules were evaluated by determination of cell viability. Human corneal fibroblasts were seeded on un-coated, YIGSR-PA coated and collagen coated wells and incubated for 72 hr. Live and dead cells were stained with calcein AM and ethidium homodimer, respectively. Live and dead cells were counted and numbers of live cells were divided to total number of cells. The viability of corneal fibroblasts were significantly higher on YIGSR-PA nanofibers compared to tissue culture plate (Figure 33). This result shows that YIGSR-PA is biocompatible with corneal fibroblast cells and can be used for further studies.

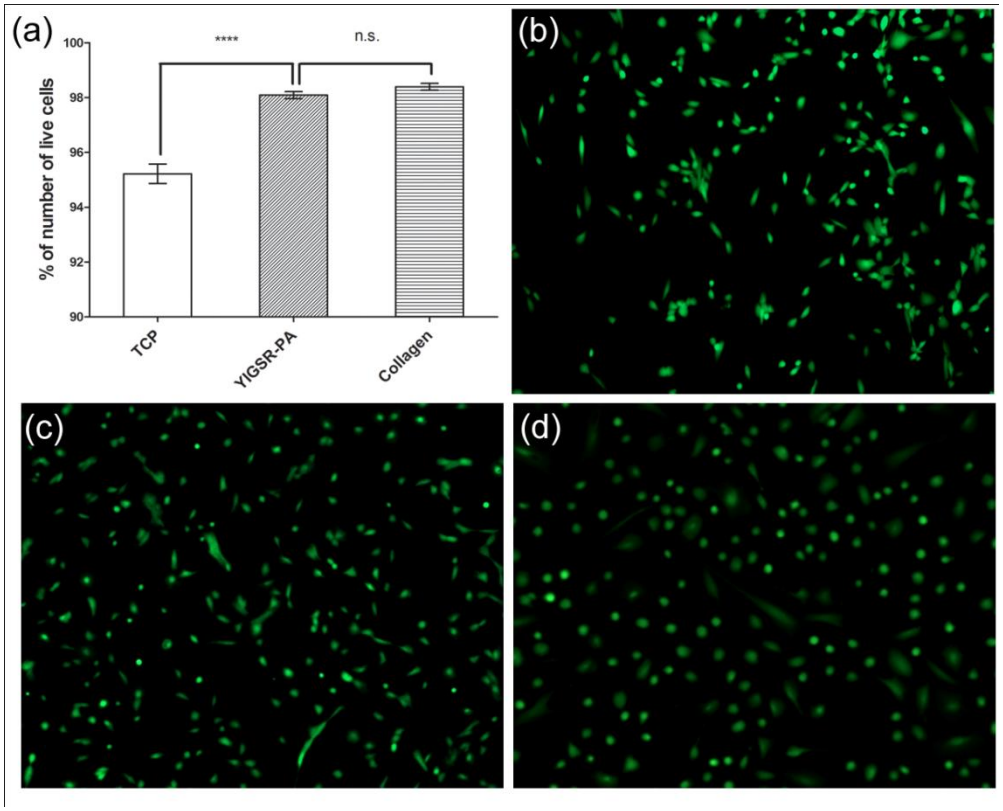

Figure 33. (a) The ratio of live cells to total number of cells representing the viability of corneal fibroblasts on TCP, YIGSR-PA coated and collagen coated surfaces. Cells were stained with Calcein AM and Ethidium Homodimer-1. Representative fluorescent images of corneal fibroblasts cultured into (b) uncoated wells, (c) YIGSR-PA coated wells and (d) collagen coated wells at 72 hours. (**** $p<0.0001$, n.s.: No Significance).

3.6.2 Cell Adhesion Assays

Adhesion and migration of corneal fibroblasts should be promoted within the PA gel injected in the stroma. To assess the adhesion of corneal fibroblast cells on the YIGSR-PA coated surface, filamentous actins and nuclei were stained with TRITC-conjugated phalloidin and TO-PRO®-3 iodide, respectively. The adhesion of cells is important because cells tend to adhere to their environment and direct their cellular processes like survival or proliferation according to the mechanical and functional characteristics of the environment that they interact with. Adhesion and spreading profiles of the corneal fibroblasts did not demonstrate a significant difference on YIGSR-PA coated wells compared to collagen coated wells or glass surface (Figure 34). This profile was also confirmed with SEM imaging of HTKs cultured on these surfaces. This result is important because adherent cells need to adhere to a surface in order to retain their viability and function. Collagen is one of the main members of the native extracellular matrix and the biocompatibility of YIGSR-PA coated surfaces can be interpreted by the similar adhesion and spreading profile observed with collagen coated surfaces.

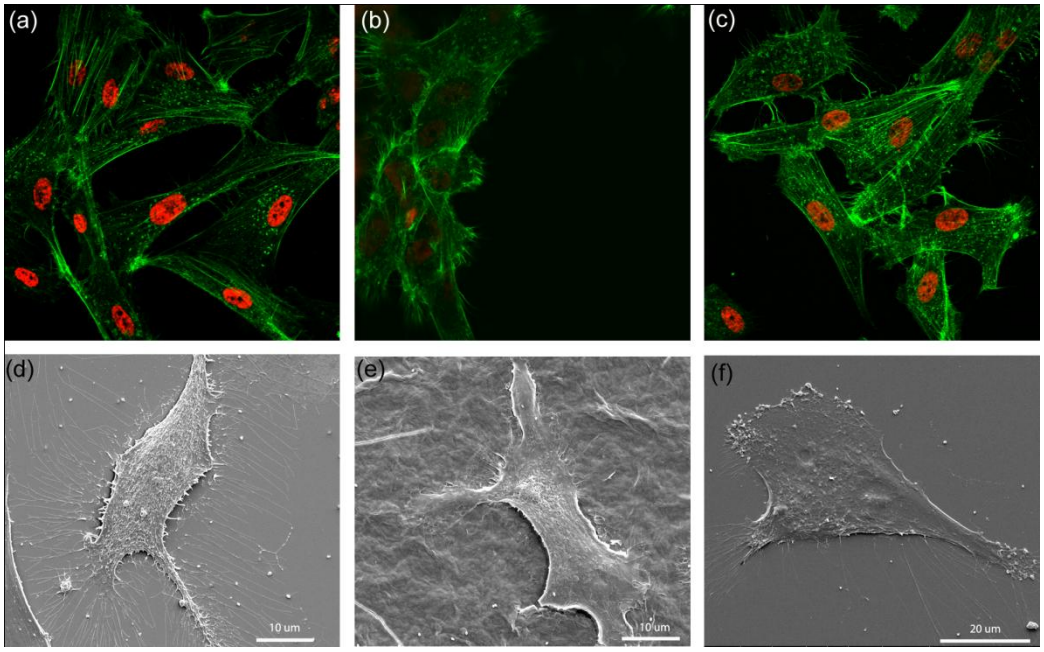

Figure 34. Spreading and cellular morphology of corneal fibroblasts acquired by staining with TRITC-conjugated phalloidin and TO-PRO®-3 iodide on (a) uncoated glass surface (63 X), (b) YIGSR-PA coated surface (63 X) and (c) collagen coated surface (63 X). SEM images of corneal fibroblasts cultured on (d) uncoated glass surface, (e) YIGSR-PA coated surface and (f) collagen coated surface.

3.6.3 Cell Proliferation on PA Gels

Maintaining the proliferation capacity of corneal fibroblasts within PA gel is crucial. The rate of increase in corneal stroma thickness, new tissue formation, mainly depends on two events: cell proliferation and synthesis of new extracellular matrix. The rate of extracellular matrix synthesis is also dependent on cell number. The proliferation capacity of corneal fibroblasts cultured on uncoated, YIGSR-PA coated and collagen coated surfaces for 72 hr was assessed with BrdU cell proliferation assay. The proliferation rate of corneal fibroblasts on YIGSR-PA coated surfaces is significantly higher than cells cultured on non-coated surfaces (Figure 35). This result shows that YIGSR-PA gels can be used further for *in vivo* studies to ensure higher proliferative capacity of human corneal fibroblasts which in turn would provide quicker recovery of corneal stroma.

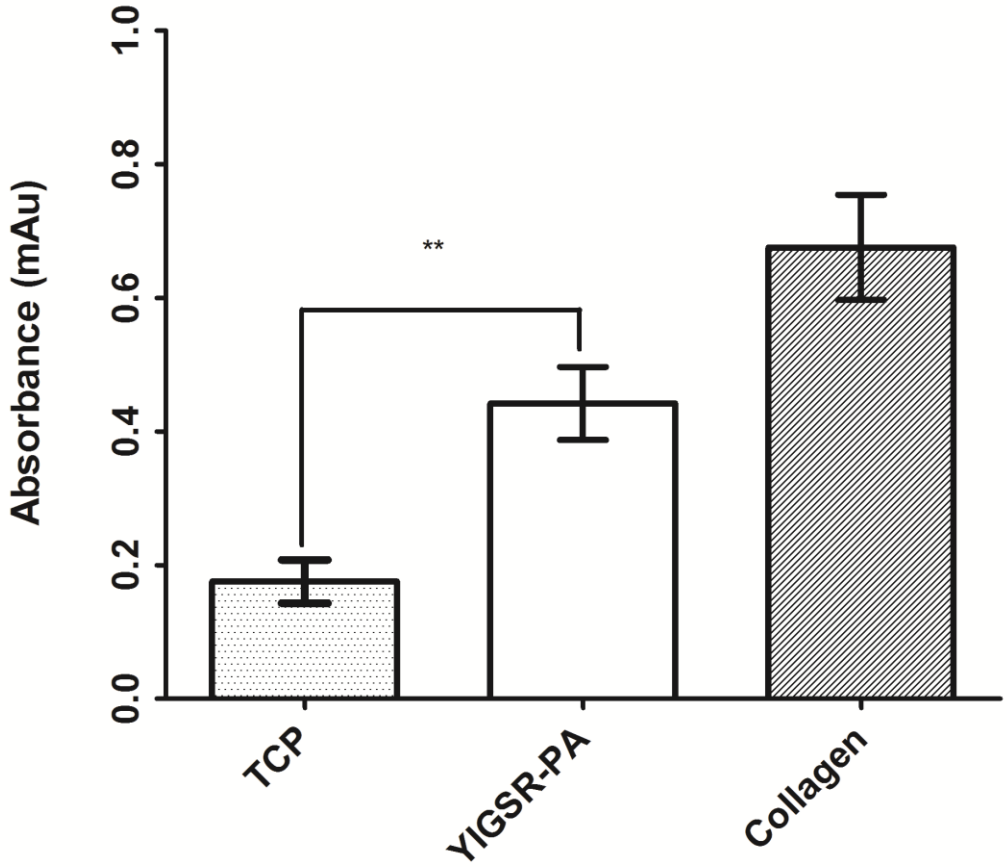

Figure 35. Evaluation of cell proliferation using 5-bromodeoxyuridine (BrdU). 2×10^4 cells/well of corneal fibroblasts were seeded on each surface placed in 24-well plates, and were cultured for 3 days. (** $p<0.003$)

Conclusion

In this chapter, we studied the utilization of “YIGSR” bioactive epitope containing peptide amphiphile molecules for corneal stroma regeneration. The effects of YIGSR-PA on biocompatibility, adhesion and proliferation of corneal fibroblast cells was assessed. The biocompatibility test suggests that corneal fibroblast cells cultured on YIGSR-PA show higher viability ratio than those cultured on tissue culture plate and there was no significant difference compared to cells cultured on collagen coating. Human corneal fibroblast cells have shown similar adhesion profiles in all test conditions. In addition to these results, corneal fibroblast cells have proliferated significantly more on YIGSR-PA than tissue culture plates. These observations suggest that YIGSR-PA can be used for *in vivo* experiments aiming regeneration of corneal stroma.

REFERENCES

1. Cui, H., M.J. Webber, and S.I. Stupp, *Self-assembly of peptide amphiphiles: from molecules to nanostructures to biomaterials.* Biopolymers, 2010. **94**(1): p. 1-18.
2. Stendahl, J.C., et al., *Intermolecular forces in the self-assembly of peptide amphiphile nanofibers.* Advanced Functional Materials, 2006. **16**(4): p. 499-508.
3. Hartgerink, J.D., E. Beniash, and S.I. Stupp, *Peptide-amphiphile nanofibers: a versatile scaffold for the preparation of self-assembling materials.* Proc Natl Acad Sci U S A, 2002. **99**(8): p. 5133-8.
4. Behanna, H.A., et al., *Coassembly of amphiphiles with opposite peptide polarities into nanofibers.* J Am Chem Soc, 2005. **127**(4): p. 1193-200.
5. Velichko, Y.S., S.I. Stupp, and M.O. de la Cruz, *Molecular simulation study of peptide amphiphile self-assembly.* J Phys Chem B, 2008. **112**(8): p. 2326-34.
6. Ganesh, S., S. Prakash, and R. Jayakumar, *Spectroscopic investigation on gel-forming beta-sheet assemblage of peptide derivatives.* Biopolymers, 2003. **70**(3): p. 346-54.
7. Paramonov, S.E., H.W. Jun, and J.D. Hartgerink, *Self-assembly of peptide-amphiphile nanofibers: the roles of hydrogen bonding and amphiphilic packing.* J Am Chem Soc, 2006. **128**(22): p. 7291-8.
8. Beniash, E., et al., *Self-assembling peptide amphiphile nanofiber matrices for cell entrapment.* Acta Biomater, 2005. **1**(4): p. 387-97.
9. Zhang, S., et al., *Spontaneous assembly of a self-complementary oligopeptide to form a stable macroscopic membrane.* Proc Natl Acad Sci U S A, 1993. **90**(8): p. 3334-8.
10. Guler, M.O., et al., *Presentation of RGDS epitopes on self-assembled nanofibers of branched peptide amphiphiles.* Biomacromolecules, 2006. **7**(6): p. 1855-1863.
11. Bull, S.R., et al., *Magnetic resonance imaging of self-assembled biomaterial scaffolds.* Bioconjug Chem, 2005. **16**(6): p. 1343-8.
12. Niece, K.L., et al., *Self-assembly combining two bioactive peptide-amphiphile molecules into nanofibers by electrostatic attraction.* J Am Chem Soc, 2003. **125**(24): p. 7146-7.
13. Silva, G.A., et al., *Selective differentiation of neural progenitor cells by high-epitope density nanofibers.* Science, 2004. **303**(5662): p. 1352-5.
14. Hartgerink, J.D., E. Beniash, and S.I. Stupp, *Self-assembly and mineralization of peptide-amphiphile nanofibers.* Science, 2001. **294**(5547): p. 1684-8.
15. Sargeant, T.D., et al., *Hybrid bone implants: Self-assembly of peptide amphiphile nanofibers within porous titanium.* Biomaterials, 2008. **29**(2): p. 161-171.
16. Tysseling-Mattiace, V.M., et al., *Self-assembling nanofibers inhibit glial scar formation and promote axon elongation after spinal cord injury.* J Neurosci, 2008. **28**(14): p. 3814-23.
17. Engler, A.J., et al., *Matrix elasticity directs stem cell lineage specification.* Cell, 2006. **126**(4): p. 677-89.

18. Ingber, D.E., *Tensegrity II. How structural networks influence cellular information processing networks.* J Cell Sci, 2003. **116**(Pt 8): p. 1397-408.
19. Ingber, D.E., *Tensegrity I. Cell structure and hierarchical systems biology.* J Cell Sci, 2003. **116**(Pt 7): p. 1157-73.
20. Schwartz, M.A. and V. Baron, *Interactions between mitogenic stimuli, or, a thousand and one connections.* Curr Opin Cell Biol, 1999. **11**(2): p. 197-202.
21. Taipale, J. and J. Keski-Oja, *Growth factors in the extracellular matrix.* FASEB J, 1997. **11**(1): p. 51-9.
22. Rosso, F., et al., *From cell-ECM interactions to tissue engineering.* J Cell Physiol, 2004. **199**(2): p. 174-80.
23. Lo, C.M., et al., *Cell movement is guided by the rigidity of the substrate.* Biophys J, 2000. **79**(1): p. 144-52.
24. Beningo, K.A. and Y.L. Wang, *Fc-receptor-mediated phagocytosis is regulated by mechanical properties of the target.* J Cell Sci, 2002. **115**(Pt 4): p. 849-56.
25. MacKintosh, F.C., J. Kas, and P.A. Janmey, *Elasticity of semiflexible biopolymer networks.* Phys Rev Lett, 1995. **75**(24): p. 4425-4428.
26. Tharmann, R., M.M. Claessens, and A.R. Bausch, *Micro- and macrorheological properties of actin networks effectively cross-linked by depletion forces.* Biophys J, 2006. **90**(7): p. 2622-7.
27. Pierschbacher, M.D. and E. Ruoslahti, *Cell attachment activity of fibronectin can be duplicated by small synthetic fragments of the molecule.* Nature, 1984. **309**(5963): p. 30-3.
28. Tsonchev, S., et al., *Phase diagram for assembly of biologically-active peptide amphiphiles.* J Phys Chem B, 2008. **112**(2): p. 441-7.
29. Krimm, S. and J. Bandekar, *Vibrational spectroscopy and conformation of peptides, polypeptides, and proteins.* Adv Protein Chem, 1986. **38**: p. 181-364.
30. Manning, M.C., M. Illangasekare, and R.W. Woody, *Circular dichroism studies of distorted alpha-helices, twisted beta-sheets, and beta turns.* Biophys Chem, 1988. **31**(1-2): p. 77-86.
31. Greenfield, M.A., et al., *Tunable mechanics of peptide nanofiber gels.* Langmuir, 2010. **26**(5): p. 3641-7.
32. Bernal, V. and P. Jelen, *Effect of Calcium Binding on Thermal Denaturation of Bovine α-Lactalbumin.* Journal of dairy science, 1984. **67**(10): p. 2452-2454.
33. Spungin, A. and S. Blumberg, *Streptomyces griseus aminopeptidase is a calcium-activated zinc metalloprotein.* European Journal of Biochemistry, 1989. **183**(2): p. 471-477.
34. Whitcher, J.P., M. Srinivasan, and M.P. Upadhyay, *Prevention of corneal ulceration in the developing world.* Int Ophthalmol Clin, 2002. **42**(1): p. 71-7.
35. Whitcher, J.P., M. Srinivasan, and M.P. Upadhyay, *Corneal blindness: a global perspective.* Bull World Health Organ, 2001. **79**(3): p. 214-21.
36. Thompson, R.W., Jr., et al., *Long-term graft survival after penetrating keratoplasty.* Ophthalmology, 2003. **110**(7): p. 1396-402.
37. Griffith, M., et al., *Functional human corneal equivalents constructed from cell lines.* Science, 1999. **286**(5447): p. 2169-72.
38. Morishige, N., et al., *Noninvasive corneal stromal collagen imaging using two-photon-generated second-harmonic signals.* J Cataract Refract Surg, 2006. **32**(11): p. 1784-91.
39. Torbet, J., et al., *Orthogonal scaffold of magnetically aligned collagen lamellae for corneal stroma reconstruction.* Biomaterials, 2007. **28**(29): p. 4268-76.

40. Hay, E.D., *Development of the vertebrate cornea.* Int Rev Cytol, 1979. **63**: p. 263-322.
41. Hogan, M.J., J.A. Alvarado, and J.E. Weddell, *Histology of the human eye; an atlas and textbook*. 1971, Philadelphia,: Saunders. xiii, 687 p.
42. Reinach, P.S. and K.S. Pokorny, *The corneal epithelium: clinical relevance of cytokine-mediated responses to maintenance of corneal health.* Arq Bras Oftalmol, 2008. **71**(6 Suppl): p. 80-6.
43. Tao, W., et al., *ETB and epidermal growth factor receptor stimulation of wound closure in bovine corneal epithelial cells.* Invest Ophthalmol Vis Sci, 1995. **36**(13): p. 2614-22.
44. Ohashi, Y., et al., *Presence of epidermal growth factor in human tears.* Invest Ophthalmol Vis Sci, 1989. **30**(8): p. 1879-82.
45. Wilson, S.E., S.A. Lloyd, and R.H. Kennedy, *Epidermal growth factor messenger RNA production in human lacrimal gland.* Cornea, 1991. **10**(6): p. 519-24.
46. Marshall, G.E., A.G. Konstas, and W.R. Lee, *Immunogold fine structural localization of extracellular matrix components in aged human cornea. I. Types I-IV collagen and laminin.* Graefes Arch Clin Exp Ophthalmol, 1991. **229**(2): p. 157-63.
47. Nakayasu, K., et al., *Distribution of types I, II, III, IV and V collagen in normal and keratoconus corneas.* Ophthalmic Res, 1986. **18**(1): p. 1-10.
48. Schermer, A., S. Galvin, and T.T. Sun, *Differentiation-related expression of a major 64K corneal keratin in vivo and in culture suggests limbal location of corneal epithelial stem cells.* J Cell Biol, 1986. **103**(1): p. 49-62.
49. Fini, M.E. and B.M. Stramer, *How the cornea heals: cornea-specific repair mechanisms affecting surgical outcomes.* Cornea, 2005. **24**(8 Suppl): p. S2-S11.
50. Muller, L.J., L. Pels, and G.F. Vrensen, *Novel aspects of the ultrastructural organization of human corneal keratocytes.* Invest Ophthalmol Vis Sci, 1995. **36**(13): p. 2557-67.
51. Zieske, J.D., *Corneal development associated with eyelid opening.* Int J Dev Biol, 2004. **48**(8-9): p. 903-11.
52. Wilson, S.E., M. Netto, and R. Ambrosio, Jr., *Corneal cells: chatty in development, homeostasis, wound healing, and disease.* Am J Ophthalmol, 2003. **136**(3): p. 530-6.
53. Jester, J.V., W.M. Petroll, and H.D. Cavanagh, *Corneal stromal wound healing in refractive surgery: the role of myofibroblasts.* Prog Retin Eye Res, 1999. **18**(3): p. 311-56.
54. Stramer, B.M., et al., *Molecular mechanisms controlling the fibrotic repair phenotype in cornea: implications for surgical outcomes.* Invest Ophthalmol Vis Sci, 2003. **44**(10): p. 4237-46.
55. Axelsson, I. and D. Heinegard, *Fractionation of proteoglycans from bovine corneal stroma.* Biochem J, 1975. **145**(3): p. 491-500.
56. Anseth, A., *Studies on corneal polysaccharides. III. Topographic and comparative biochemistry.* Exp Eye Res, 1961. **1**: p. 106-15.
57. Blochberger, T.C., et al., *cDNA to chick lumican (corneal keratan sulfate proteoglycan) reveals homology to the small interstitial proteoglycan gene family and expression in muscle and intestine.* J Biol Chem, 1992. **267**(1): p. 347-52.

58. Corpuz, L.M., et al., *Molecular cloning and tissue distribution of keratocan. Bovine corneal keratan sulfate proteoglycan 37A.* J Biol Chem, 1996. **271**(16): p. 9759-63.
59. Liu, C.Y., et al., *The cloning of mouse keratocan cDNA and genomic DNA and the characterization of its expression during eye development.* J Biol Chem, 1998. **273**(35): p. 22584-8.
60. Funderburgh, J.L., et al., *Mimecan, the 25-kDa corneal keratan sulfate proteoglycan, is a product of the gene producing osteoglycin.* J Biol Chem, 1997. **272**(44): p. 28089-95.
61. Bettelheim, F.A. and B. Plessy, *The hydration of proteoglycans of bovine cornea.* Biochim Biophys Acta, 1975. **381**(1): p. 203-14.
62. Chakravarti, S., et al., *Collagen fibril assembly during postnatal development and dysfunctional regulation in the lumican-deficient murine cornea.* Dev Dyn, 2006. **235**(9): p. 2493-506.
63. Rada, J.A., P.K. Cornuet, and J.R. Hassell, *Regulation of corneal collagen fibrillogenesis in vitro by corneal proteoglycan (lumican and decorin) core proteins.* Exp Eye Res, 1993. **56**(6): p. 635-48.
64. Borcherding, M.S., et al., *Proteoglycans and collagen fibre organization in human corneoscleral tissue.* Exp Eye Res, 1975. **21**(1): p. 59-70.
65. Scott, J.E., *Proteoglycan: collagen interactions and corneal ultrastructure.* Biochem Soc Trans, 1991. **19**(4): p. 877-81.
66. Karring, H., et al., *Proteomic analysis of the soluble fraction from human corneal fibroblasts with reference to ocular transparency.* Mol Cell Proteomics, 2004. **3**(7): p. 660-74.
67. Ethier, C.R., M. Johnson, and J. Ruberti, *Ocular biomechanics and biotransport.* Annu Rev Biomed Eng, 2004. **6**: p. 249-73.
68. Maurice, D.M., *The location of the fluid pump in the cornea.* J Physiol, 1972. **221**(1): p. 43-54.
69. Ruberti, J.W. and S.D. Klyce, *NaCl osmotic perturbation can modulate hydration control in rabbit cornea.* Exp Eye Res, 2003. **76**(3): p. 349-59.
70. Zieske, J.D., et al., *Basement membrane assembly and differentiation of cultured corneal cells: importance of culture environment and endothelial cell interaction.* Exp Cell Res, 1994. **214**(2): p. 621-33.
71. Orwin, E.J. and A. Hubel, *In vitro culture characteristics of corneal epithelial, endothelial, and keratocyte cells in a native collagen matrix.* Tissue Eng, 2000. **6**(4): p. 307-19.
72. Joyce, N.C., et al., *Cell cycle protein expression and proliferative status in human corneal cells.* Invest Ophthalmol Vis Sci, 1996. **37**(4): p. 645-55.
73. Joyce, N.C., et al., *Expression of cell cycle-associated proteins in human and rabbit corneal endothelium in situ.* Invest Ophthalmol Vis Sci, 1996. **37**(8): p. 1566-75.
74. Bohnke, M., P. Eggli, and K. Engelmann, *Transplantation of cultured adult human or porcine corneal endothelial cells onto human recipients in vitro. Part II: Evaluation in the scanning electron microscope.* Cornea, 1999. **18**(2): p. 207-13.
75. Engelmann, K., D. Drexler, and M. Bohnke, *Transplantation of adult human or porcine corneal endothelial cells onto human recipients in vitro. Part I: Cell culturing and transplantation procedure.* Cornea, 1999. **18**(2): p. 199-206.

76. Chen, K.H., D. Azar, and N.C. Joyce, *Transplantation of adult human corneal endothelium ex vivo: a morphologic study.* Cornea, 2001. **20**(7): p. 731-7.
77. Hicks, C.R., et al., *Corneal replacement using a synthetic hydrogel cornea, AlphaCor: device, preliminary outcomes and complications.* Eye (Lond), 2003. **17**(3): p. 385-92.
78. Bleckmann, H. and S. Holak, *Preliminary results after implantation of four AlphaCor artificial corneas.* Graefes Arch Clin Exp Ophthalmol, 2006. **244**(4): p. 502-6.
79. Chow, C.C., et al., *Clinicopathologic correlation of explanted AlphaCor artificial cornea after exposure of implant.* Cornea, 2007. **26**(8): p. 1004-7.
80. Strampelli, B. and V. Marchi, *[Osteo-odonto-keratoprosthesis].* Ann Ottalmol Clin Ocul, 1970. **96**(1): p. 1-57.
81. White, J.H. and O. Gona, *"Proplast" for keratoprosthesis.* Ophthalmic Surg, 1988. **19**(5): p. 331-3.
82. Blencke, B.A., et al., *[Study on the use of glass ceramics in osteo-odonto-keratoplasty].* Ophthalmologica, 1978. **176**(2): p. 105-12.
83. Caiazza, S., G. Falcinelli, and S. Pintucci, *Exceptional case of bone resorption in an osteo-odonto-keratoprosthesis. A scanning electron microscopy and X-ray microanalysis study.* Cornea, 1990. **9**(1): p. 23-7.
84. Lanza, R.P., R.S. Langer, and J. Vacanti, *Principles of tissue engineering*. 3rd ed. 2007, Amsterdam ; Boston: Elsevier / Academic Press. xxvii, 1307 p.
85. Ruberti, J.W. and J.D. Zieske, *Prelude to corneal tissue engineering - Gaining control of collagen organization.* Progress in Retinal and Eye Research, 2008. **27**(5): p. 549-577.
86. Graf, J., et al., *A pentapeptide from the laminin B1 chain mediates cell adhesion and binds the 67,000 laminin receptor.* Biochemistry, 1987. **26**(22): p. 6896-900.
87. Bellamkonda, R., J.P. Ranieri, and P. Aebischer, *Laminin oligopeptide derivatized agarose gels allow three-dimensional neurite extension in vitro.* J Neurosci Res, 1995. **41**(4): p. 501-9.
88. Li, F., et al., *Cellular and nerve regeneration within a biosynthetic extracellular matrix for corneal transplantation.* Proc Natl Acad Sci U S A, 2003. **100**(26): p. 15346-51.
89. Shah, R.N., et al., *Supramolecular design of self-assembling nanofibers for cartilage regeneration.* Proc Natl Acad Sci U S A, 2010. **107**(8): p. 3293-8.
90. Mata, A., et al., *Bone regeneration mediated by biomimetic mineralization of a nanofiber matrix.* Biomaterials, 2010. **31**(23): p. 6004-12.
91. Chow, L.W., et al., *A bioactive self-assembled membrane to promote angiogenesis.* Biomaterials, 2011. **32**(6): p. 1574-82.
92. Ruoslahti, E., *RGD and other recognition sequences for integrins.* Annu Rev Cell Dev Biol, 1996. **12**: p. 697-715.
93. Massia, S.P., S.S. Rao, and J.A. Hubbell, *Covalently immobilized laminin peptide Tyr-Ile-Gly-Ser-Arg (YIGSR) supports cell spreading and co-localization of the 67-kilodalton laminin receptor with alpha-actinin and vinculin.* J Biol Chem, 1993. **268**(11): p. 8053-9.
94. Iwamoto, Y., et al., *Synthetic pentapeptide from the B1 chain of laminin promotes B16F10 melanoma cell migration.* J Cell Physiol, 1988. **134**(2): p. 287-91.

95. Jester, J.V., et al., *Myofibroblast differentiation of normal human keratocytes and hTERT, extended-life human corneal fibroblasts.* Invest Ophthalmol Vis Sci, 2003. **44**(5): p. 1850-8.
96. Duan, X., et al., *Biofunctionalization of collagen for improved biological response: scaffolds for corneal tissue engineering.* Biomaterials, 2007. **28**(1): p. 78-88.
97. Hara, M., et al., *Production of interferon-beta by NB1-RGB cells cultured on peptide-lipid membranes.* Cytotechnology, 2003. **42**(1): p. 13-20.
98. Boateng, S.Y., et al., *RGD and YIGSR synthetic peptides facilitate cellular adhesion identical to that of laminin and fibronectin but alter the physiology of neonatal cardiac myocytes.* Am J Physiol Cell Physiol, 2005. **288**(1): p. C30-8.
99. Dana, A., et al., *Interfiber interactions alter the stiffness of gels formed by supramolecular self-assembled nanofibers.* Soft Matter, 2011. **7**(7): p. 3524-3532.